polynomials form a complete basis set we may solve for $\rho(x)/\rho^T(x)$ in terms of them. Thus

$$\rho(x) = \sum_{j=0}^{\infty} c_j H_j(x)(2\pi)^{1/2} \exp(-\tfrac{1}{2}x^2) \quad (78)$$

where $c_j = (1/j!)\int_{-\infty}^{\infty}\rho(x)H_j(x)\,dx$. This expansion though is a moment expansion.

Let us define

$$\rho_n(x) = \sum_{j=0}^{n} c_j H_j(x)(2\pi)^{1/2} \exp(-\tfrac{1}{2}x^2) \quad (79)$$

Claim. $\mu_i(\rho_m) = \mu_i(\rho)$ for all $m \geq i$.

Proof.

$$\mu_i(\rho) = \int x^i\rho(x)\,dx = \int x^i \sum_{j=0}^{m} c_j H_j(x)(2\pi)^{1/2} \exp(-\tfrac{1}{2}x^2)\,dx \quad (80)$$

for all $m \geq i$. In turn this

$$= \int x^i \sum_{j=0}^{i} c_j H_j(x)(2\pi)^{1/2} \exp(-\tfrac{1}{2}x^2)\,dx = \mu_i(\rho_m) \quad (81)$$

The equivalence follows from the first footnote given in Appendix section III.

Hence, for arbitrary ρ^T, the problem reduces to finding the correct polynomial basis set. These though are nothing more than the $P_j(x)$ polynomials which correspond to the DOS ρ^T.

The Moments Method and Elemental Structures

Jeremy K. Burdett*[1] and Stephen Lee

Contribution from the Department of Chemistry, The University of Chicago, Chicago, Illinois 60637. *Received May 21, 1984*

Abstract: The ability of the method of moments to make qualitative predictions of structure is tested on the structures of main group and transition elements. Trends due to the presence of rings and bond angles of various sizes are discussed.

I. Introduction

In the previous[2] paper paper in this issue, we presented a simple method for estimating the electronic energy of solids by using a one-electron tight-binding model based on the Hückel approximation. This method in its simplest form expresses the energy difference between two structures in terms of the earliest disparate moment of their respective energy density of states (DOS). In Figure 1a we show the energy difference curves expected for a pair of structures as a function of band filling, X ($0 \leq X \leq 1$) where the first dominant moment difference occurs in μ_m (m = 2–6). Sometimes, if there is a "tail" on the bonding side of the density of states (arising perhaps via the inclusion of s and p orbitals in the bonding picture), then the nodes in these curves shift to smaller X. The convention used in Figure 1 is that when the curves have positive values, then that structure with the largest $|\mu_m|$ is the more stable. (We assume odd moments are negative in this statement.) Some generalizations are interesting to describe.

(1) Low moments are more important than higher moments in controlling the form of the energy difference curve. Real attention should be paid to μ_3 and μ_4.

(2) For two structures A and B, let us put $|\mu_3(A)| > |\mu_3(B)|$ and assume both $\mu_3(A)$ and $\mu_3(B)$ to be negative. Then, with reference to Figure 1, A will be the favored structure below the half-filled band and B will be favored above the half-filled band. The crossing point itself lies below the half-filled band for the $\Delta E_3(X)$ curves of the previous paper in this issue where we compared the energetics of the 3-ring within the 3-tree with the 3-tree itself. (In general the crossing points in the $\Delta E(X)$ curves will depend on the exact form of the densities of states for the two systems as discussed further in (5).)

(3) If $\mu_3(A) = \mu_3(B)$ but $\mu_4(A) > \mu_4(B)$, then B is favored at the half-filled band while A is favored at lower and higher band fillings.

(4) Systems with a large (negative) μ_5 are energetically stabilized just above the half-filled band. A large (positive) μ_6 stabilizes systems at the half-filled point itself.

(5) The presence of "tails" in the DOS which trail toward the bonding edge limit shift the crossing points of Figure 1a toward smaller X (Figure 1b). Such tails may be anticipated by the presence of large and negative values of μ_3. (If a large tail exists, then μ_4, μ_5, etc., should be large too of course. If μ_3 is large but μ_4 small, then this implies no strong tail.)

In this paper we wish to discuss the usefulness of these rules. Clearly we need to find out if the early moments are easy to determine (without the aid of a computer) and if the rules accurately predict Hückel energetics. The whole approach of course relies on the utility of one-electron, Hückel-based calculations themselves. There are many areas where such an approach does not accurately reflect electronic energy. Bond length changes and coordination number variations are two of them. We shall therefore in general avoid examples which are inappropriate for the Hückel or extended Hückel models.

II. Rings

The Hückel model of the π manifold in benzene (for example) is well-known.[3] It predicts a stabilization of benzene relative to other unsaturated carbon configurations—the so-called resonance energy. In terms of the moments approach[4] this result is due to both the fact that each carbon atom contributes one electron to the π system (a half-filled "band") and the presence in benzene of the six-membered ring. In the previous paper in this issue, we showed how at the half-filled point the six-membered ring was stabilized with respect to the simple tree. Similarly cyclobutadiene is viewed as an unfavorable arrangement by using traditional Hückel ideas. Analogously in the moments approach, 4-rings are destabilized at the half-filled point. However, as we will see frequently in this paper 6-rings are destabilized at other band

(1) Camille and Henry Dreyfus Teacher-Scholar.
(2) Burdett, J. K.; Lee, S. *J. Am. Chem. Soc.*, preceding paper in this issue.
(3) (a) Hückel, E. *Z. Phys.* **1931**, *70*, 204; **1932**, *76*, 628. (b) Streitweiser, A. "Molecular Orbital Theory for Organic Chemists"; Wiley: New York, 1961. (c) Heilbronner, E.; Bock, H. "The HMO Model and its Application"; Wiley: New York, 1976.
(4) We derive the Hückel eigenvalue spectra of some small conjugated hydrocarbons in: Burdett, J. K.; Lee, S.; Sha, W. C. *Croat. Chim. Acta* **1984**, *57*, 1193.

0002-7863/85/1507-3063$01.50/0

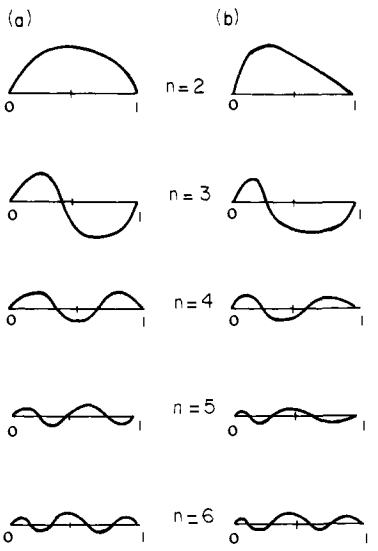

Figure 1. Energy difference curves as a function of band filling between two structures whose first disparate moment is μ_n, where n is shown in the central column. The convention used is that when the curves have positive values, the structure with the larger $|\mu_n|$ is more stable: (a) the case where no tail exists in the DOS, (b) the result of a tail in the DOS at the bonding edge. By tail it is meant a DOS which near its edge (i.e., most bonding or antibonding states) a wide span of energy levels must be crossed before the accumulated area in the DOS is significant.

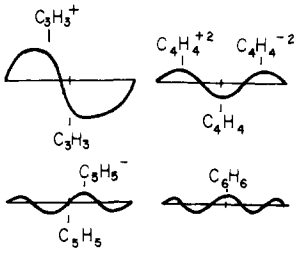

Figure 2. Comparison with Huckel $4n + 2$ rule. We have placed on the curves of Figure 1 at the proper electron counts the various carbon planar rings. The results may be seen to encompass the Hückel $4n + 2$ rule.

fillings just as 4-rings are stabilized at points away from the half-filled position. Such a result is inherent in Hückel's $4n + 2$ rule. Notice in Figure 2 where we have indicated on the set of curves of Figure 1a the relevant "band fillings" for $C_3H_3^+$, $C_4H_4^{2+}$, $C_4H_4^{2-}$, and $C_5H_5^-$ that the presence of the charge (whether positive or negative) has shifted the band filling away from $X = {}^1/_2$, an unfavorable one for these rings. The result has been that all of these species in obeying Hückel's $4n + 2$ rule have ended up in a region of stability with respect to the simple tree.

The concepts we have described include, as a special case for $X = 0.5$, results from graph theory which allow computation of the resonance energies of conjugated hydrocarbons.[5-9] In this approach the resonance energy is written as

$$\mathrm{RE} = \frac{1}{K}[\sum_{m=1}(a_m R_m + b_m Q_m)] \qquad (1)$$

(5) (a) Randic, M. *J. Am. Chem. Soc.* **1977**, *99*, 444. (b) Randic, M. *Mol. Phys.* **1977**, *34*, 849. (c) Gutman, I.; Randic, M. *Chem. Phys.* **1979**, *41*, 265.
(6) See: Trinajstic, N. "Graph Theory"; CRC Press: Boca Raton, FL, 1983.
(7) (a) Herndon, W. C.; Ellzey, M. L. *J. Am. Chem. Soc.* **1976**, *96*, 6631. (b) Herndon, W. C. *Isr. J. Chem.* **1980**, *20*, 270.
(8) (a) Gutman, I.; Trinajstic, N. *Chem. Phys. Lett.* **1973**, *20*, 257. (b) Yates, K. "Hückel Molecular Orbital Theory"; Academic Press: New York, 1978.
(9) Self-returning random walks have been used to characterize structures too. See Randic, M. *J. Comput. Chem.* **1980**, *1*, 386; *Int. J. Quant. Chem.* **1980**, *1*, 386.

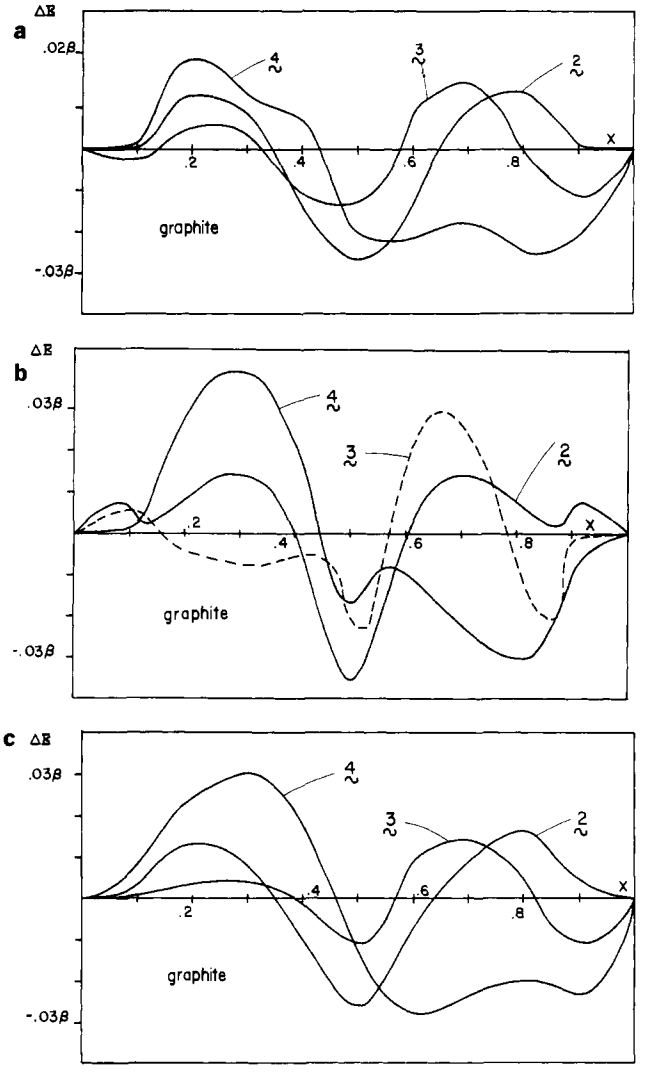

Figure 3. Differences in energy of stabilization by band filling for the π network in three-coordinate planar nets. Differences drawn are those between the **4**, **3**, and **2** structures and the graphite structure. Thus the structure whose difference curve has the highest value for a given electron count is the most stable for that electron count. When all curves are beneath the x axis, graphite is the most stable: (a) the equivalent of a full band calculation using the continued fraction method[2] using the first 30 moments, (b) the second order Q polynomial approximation,[2] and (c) approximation where we have mimicked the first six moments of each of these structures by forming a linear combination of the appropriate 3-tree DOS.[2] Finally β denotes the H_{ij} linking pπ orbitals on neighboring carbon atoms.

Table I. Planar Nets

	ScB_2C_2	graphite	CaB_2C_2	3-9
	a. Moments (in β)			
μ_2	3	3	3	3
μ_3	0	0	0	1.5
μ_4	15	15	17	15
μ_5	2.5	0	0	15
μ_6	87	93	111	88.5
μ_7	38.5	0	0	126
μ_8	545	639	773	567
	b. Moments (in standard form)			
μ_2	1.0000	1.0000	1.0000	1.0000
μ_3	0	0	0	-0.2887
μ_4	1.6667	1.6667	1.8889	1.6667
μ_5	-0.1604	0	0	-0.9623
μ_6	3.2222	3.4444	4.1111	3.2778
μ_7	-0.8233	0	0	-2.6943
μ_8	6.7284	7.8889	9.5432	7.0000

Table II. Ring Moments

	3-ring	4-ring	90° chain	5-ring	108° chain	6-ring	120° chain
μ_2	1.402	1.402	1.402	1.402	1.402	1.402	1.402
μ_3	-2.312	-0.996	-0.996	-0.996	-0.996	-0.996	-0.996
μ_4	9.788	7.706	6.789	6.041	6.041	5.627	5.627
μ_5				-9.381	-8.868	-8.342	-8.342
μ_6						30.944	29.686

Table III. $\sigma + \pi$ Planar Nets

	moments[a] (in standard form)[b]		
	ScB_2C_2	graphite	CaB_2C_2
μ_2	1.0000	1.0000	1.0000
μ_3	-0.5011	-0.5005	-0.5005
μ_4	2.5921	2.5610	2.8591
μ_5	-3.0356	-2.9034	-3.2161
μ_6	9.5191	9.2144	11.5815
μ_7	-15.8817	14.6572	-18.3093
μ_8	41.4080	38.8155	54.0805

[a] Only first nearest-neighbor interactions have been considered. Second and third nearest-neighbor effects are nevertheless important. [b] Is not equal to unity.

where a_m and b_m are the number of conjugated (closed) circuits of length $4m + 2$ and $4m$, respectively, for each of the individual Kekulē structures of the molecule (K in total). R_m and Q_m are obtained[5] via a parameterization process. All R_m are positive (stabilizing), and all Q_m are negative (destabilizing). As m increases, they drop off sharply in magnitude. These results are in accord with our treatment which gives $\Delta E_{odd}(0.5) = 0$, $\Delta E_{even}(0.5) > 0$, for even $= 4m + 2$, and $\Delta E_{even}(0.5) < 0$ for even $= 4m$.

In viewing Hückel theory in this topological fashion, it is clear that such a stabilization is expected for all planar carbon networks which contain 6-rings. An obvious solid-state example is the 6^3 net of graphite (**1**). By analogy with the molecular examples

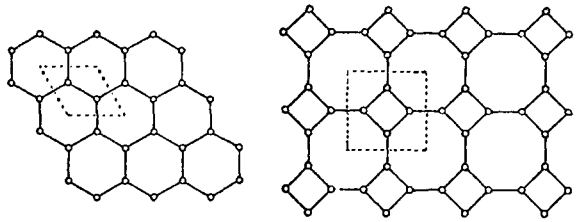

1 2

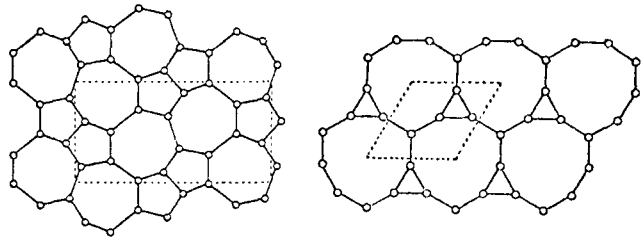

3 4

above it is interesting to compare the electronic stability of this net with other three-coordinate nets which contain rings of other sizes. **2** shows the 48^2 net found in the nonmetal part of the CaB_2C_2 system,[10] and **3** shows the net formed by the nonmetals in ScB_2C_2.[11] **4** shows a net which corresponds to no known species. As all these structures are three-coordinate, the earliest possible divergence of their moments occurs at μ_3. For the π manifolds of such planar systems, where the orbital interaction integrals (Hückel β) are independent of angle, **4**, **3**, and **2** will differ from graphite in their third, fourth, and fifth moments, respectively.

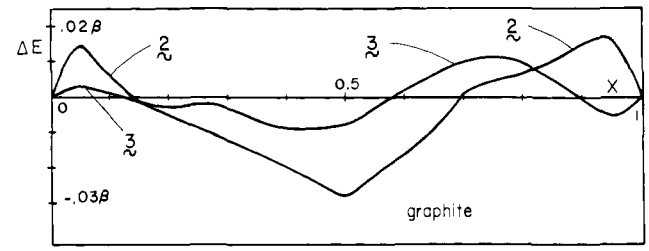

Figure 4. Differences in energy of stabilization by band filling for the $\sigma + \pi$ network in three-coordinate planar nets. See caption of Figure 3 for conventions used and Appendix section II for details of the calculation. The numerical computation used the first 30 moments.

This is shown numerically in Table I. Using the rules described in section **I**, we expect **4** to have the largest π energy below the half-filled band, **1** to be best near the half-filled band, **3** to be best above (but near) the half-filled band, while **2** to be best near the filled band. Figure 3 shows two numerical estimates of the energy differences by using the early moments of these systems and the actual result from a complete calculation. All of them share the features we have just described. Thus, graphite satisfyingly is predicted to be the most stable alternative at the half-filled point. The structure of ScB_2C_2 is made up of BC sheets with the arrangement shown in **3**. Assuming that the scandium atom which lies between these sheets contributes three electrons to this net, then there are a total of five π electrons per formula unit (i.e., a $B_2C_5^{3-}$ sheet).[12] In this case $X = 0.625$, and indeed from the curves of Figure 3 this is calculated to be the most stable structure at this point. The 48^2 sheet (**2**) in CaB_2C_2, however, is isoelectronic with graphite itself ($B_2C_2^{2-}$). This structure is predicted to be unstable at this point relative to graphite. However, remember our arguments so far really only apply to the case of the elemental structures themselves. Recall too that the molecule cyclobutadiene may be stabilized in the square structure by the attachment of donor and acceptor groups ("push–pull" cyclobutadienes). Also the square molecules $B_2X_2R_4$ (X = N and P) are quite stable. We will return to this point later.

It is of interest to ask at this stage whether it is possible by intercalation of graphite with electron donors to induce a switch in structure at a critical value of the intercalate concentration. **5** shows perhaps the simplest geometrical motion which would achieve this. It involves breaking and making one-sixth of the

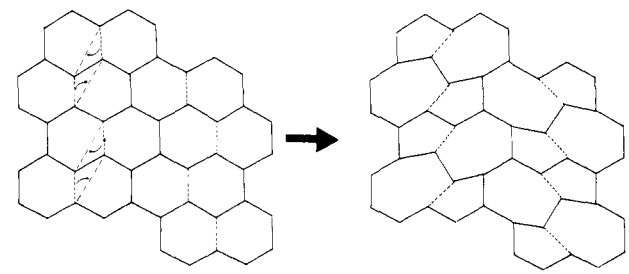

5

(10) (a) Breant, T.; Pensec, D.; Bauer, J.; Debuigne, J. *C. R. Hebd. Seances Acad. Sci., Ser. C* **1978**, *287*, 261. (b) Bauer, J.; Bars, O. *Acta Cryst. B* **1980**, *36*, 1540.

(11) Smith, G. S.; Johnson, A.; Nordine, P. C. *Acta Cryst.* **1965**, *19*, 668.

(12) Our discussion centers around the assumption that the Sc atoms are present in the lattices as Sc^{III} and that this is the driving force behind the observed structure. Another viewpoint is that the Sc is present as Sc^{II} but that the metal atom size requires the presence of seven-membered rings—in other words, a "steric" argument. In this paper we shall use the moments method to understand the shapes of the energy difference curves we calculate for various pairs of structures. Whether we get "the right answer for the wrong reasons" is a separate problem, and we will leave it for elsewhere (Burdett, J. K.; Canadell, E., unpublished results).

Table IV. Known Elemental Structures of Groups 13 and 14

13		14	
B	tetragonal-50	C	graphite
	rhombohedral-12		diamond (hexagonal and cubic)
	rhombohedral-105		
Al	fcc	Si	diamond
	hcp		white tin
	face-centered tetragonal		γ-Si
			Si(III)
Ga	α-Ga	Ge	diamond
	γ-Ga (metastable)		γ-Ge
			white tin
In	indium	Sn	diamond (grey tin)
			white tin
Tl	fcc	Pb	fcc
	hcp		
	bcc (?)		

linkages of the net. Such a process would probably be energetically unfavorable.

Bonding of the π-type, however, is not the dominant energetic feature of these systems—there are after all more orbitals involved in the σ framework. Furthermore, these σ orbitals have better overlap. There are several differences between the σ and π frameworks.

(1) As $H_{ss} \neq H_{pp}$, we must now include nonzero diagonal elements in the Hückel Hamiltonian (i.e., we cannot set both H_{pp} and H_{ss} equal to zero). These correspond to closed walks of length 1.

(2) In enumerating the walks necessary for the generation of the moments, it is no longer sufficient just to state between which atoms the walk took place. It is essential to specify the orbitals as well. This becomes complex rather rapidly. For instance, in cyclobutadiene, as there are three σ-manifold orbitals situated at each carbon atom, there are a total of $3^4 = 81$ possible σ-type paths of length 4 to be considered, each of which extends all the way around the ring.

(3) Bond angles are important, as overlap integrals and therefore interatomic interaction integrals are angle-dependent.

All these added complications, however, do not alter the presence of three-membered rings in **4**, four-membered rings in **2**, five-membered rings in **3**, and six-membered rings in **1**. The rings may therefore remain the dominant structural features in these systems. A new possibility does emerge, however. In **6** and **7** we show two triangles, each populated with a different set of p orbitals. Solution of the eigenvalue problem leads to two

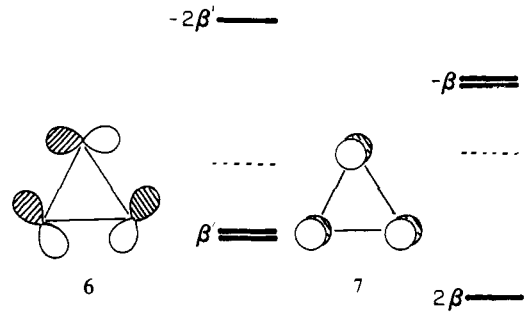

different but related energy level patterns. **6** gives rise to two bonding and one antibonding level, while in **7** the situation is reversed. The essential difference between the two systems is that in **6**, irrespective of how the relative orbital phases are drawn, there are an odd number of antibonding interactions, while in **7** there are an even (or zero) number. **6** is generally called a Möbius 3-ring and **7** a Hückel 3-ring (see ref 8b).

This distinction can be made for rings of arbitrary size. Each interaction integral linking bonded atoms is included in the weight of a given walk with a negative sign (i.e., $\beta < 0$) if the overlap integral is positive. If the net phase of the path around an m-ring is $(-1)^m$, the m-ring is a Hückel one. If the net phase is $(-1)^{m+1}$,

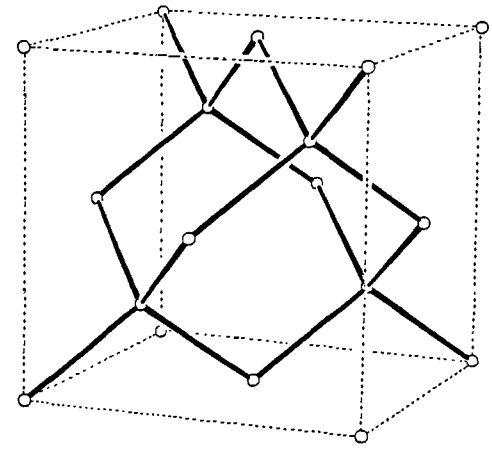

Figure 5. Cubic unit cell of cubic diamond.

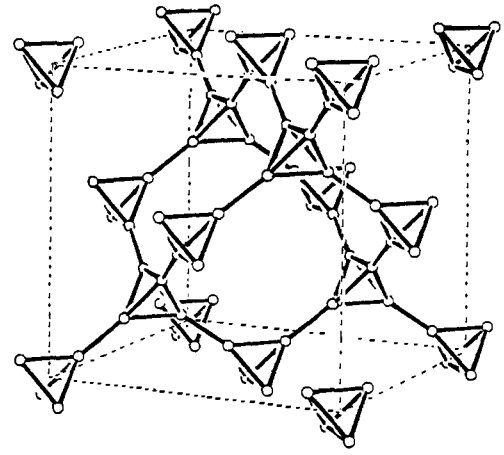

Figure 6. Cubic unit cell of tetrahedral diamond.

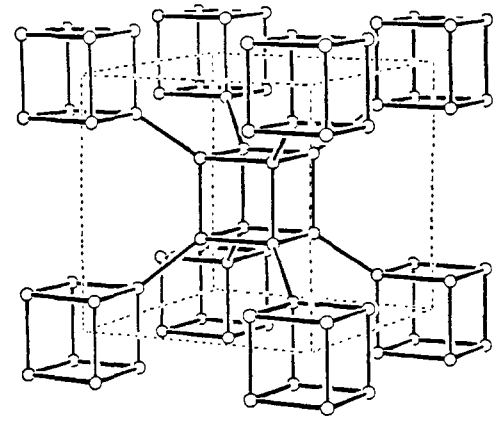

Figure 7. Cubic unit cell of supercubane.

the m-ring is Möbius. Thus, for odd rings of the same strength (i.e., equal values of β between the corresponding orbitals)

$$\mu_m(\text{Möbius } m\text{-ring}) = -\mu_m(\text{Hückel } m\text{-ring}) \quad (2)$$

For even-membered rings, complete walks around the ring only make up a part of μ_m. So for m-rings (m = even)

$$|\mu_m(\text{Möbius})| < |\mu_m(\text{Hückel})| \quad (3)$$

When considering the effect rings have on the σ DOS, we will naturally find some orbitals which interact to give a Möbius contribution and other sets of orbitals which interact in a Hückel fashion. We are interested in the overall effect of the ring, where all possible paths of a given length are summed. Thus, if there are more and stronger Hückel closed paths than Möbius paths, we may take the net effect of the ring to be a Hückel one. In Table II we assess the moments of planar three-, four-, five-, and

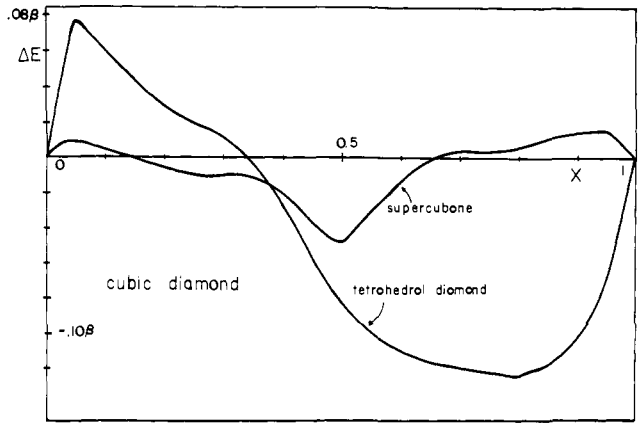

Figure 8. Differences in energy of stabilization by band filling for four-coordinate nets. See caption of Figure 3 for conventions used (here the role of graphite has been replaced by cubic diamond) and Appendix section II for details of the calculation. The calculation uses the first 30 moments.

six-membered rings. In order to determine the effect of the orbitals of the ring, we need to compare the moments with those of an infinite chain with identical local geometry. A Möbius m-ring will have a smaller mth moment than the corresponding open chain. A Hückel m-ring will have a larger mth moment. We find in every case that the net interaction is a Hückel one. We therefore expect the same qualitative trends that appeared for the pure π manifold to reappear in the $\sigma + \pi$ DOS. One change we should expect is a shift of the early nodes of the energy difference curve toward the empty band limit. This will arise simply because μ_3 is no longer equal to zero—a direct result of the fact that $H_{ss} \neq H_{pp}$. Since μ_3 is large and negative (Table II), a tail should appear toward the bonding edge and the ΔE curve should become more like the one in Figure 1b. The results of a complete numerical Hückel calculation employing both s and p orbitals are shown in Figure 4 and some of the early moments shown in Table III (see the previous paper in this issue for our usage of the label "Hückel"). The curve of Figure 4 is in good agreement with our predictions even to the anticipated downshift of the nodes.

It is perhaps surprising that all this works out so well. For instance, the seemingly vital fact that the π manifold lies in the center of the $\sigma + \pi$ band while the edges are purely σ-based has not been taken into account. Apparently the π manifold is less strongly bonding than the σ portion and can only "fine tune" the $\sigma + \pi$ ΔE curve.

III. Structures from Groups 13 and 14

There are at least[13] ten known group 13 elemental structure types and at least six known group 14 ones (Table IV).

With the exception of elemental lead, which we consider later in this paper, the chief difference between the elemental structures of groups 13 and 14 lies in the presence of 3-rings in the former and the presence of 6-rings (or at least the absence of 3- and 4-rings) in group 14. Let us first compare the well-known cubic diamond structure (Figure 5) with some possible alternatives which contain four-coordinate centers. Two hypothetical systems are shown in Figures 6 and 7. The first, "tetrahedral" diamond contains three-membered rings and is generated simply by locating tetrahedra at the nodes of the diamond lattice. The second, "supercubane" is obtained by locating cubes of atoms at the nodes of the bcc lattice. The structures of Figures 6, 7, and 5 are then dominated by the presence of three-, four-, and six-membered rings, respectively. From the diagram of Figure 1, we then expect cubic diamond to be most stable at the half-filled band (elemental carbon), supercubane to be most stable near the filled band, and tetrahedral diamond to be most stable near the empty band. In

(13) See, for example: Donahue, J. "The Structures of the Elements"; Wiley: New York, 1974.

Table V. Four-Coordinate Nets

	moments (in standard form)		
	diamond	tetrahedrons arranged in diamond fashion	cubes arranged in bcc fashion
μ_2	1.0000	1.0000	1.0000
μ_3	−0.4729	−1.3196	−0.4729
μ_4	2.5842	4.4399	3.0399
μ_5	−2.8458	−11.2657	−3.3118
μ_6	9.6623	32.4163	14.0122
μ_7	−15.1916	−90.4876	−21.9882

Figure 8 we can see that this is just what a full three-dimensional band-structure calculation shows. (The interatomic distances to nearest neighbors were kept equal in all three calculations.) Moments for these structures are given in Table V.

These predictions differ from more traditional arguments based on "ring strain" effects[14] in that the "strained" arrangements of Figures 6 and 7 are actually energetically favored at certain electron counts and the "unstrained" arrangement of Figure 5 is energetically disfavored at some electron counts. In this aspect, our approach resembles the traditional bonding concepts used for the π systems of unsaturated hydrocarbons (aromatic and antiaromatic behavior) described in section II. The possibility of σ aromaticity has been considered before and the Dewar–Zimmerman arguments[15] have played a valuable role in the development of organic chemistry. Dewar in his work[15a] in this area acknowledged the destabilizing effect of the σ 3-ring in cyclopropane but suggested that the molecule may have a σ-aromatic stabilization as a result of, in our language, the stabilizing effect at the half-filled point of the walk of length 6 which connects the six sp^3 hybrid orbitals of the σ manifold. As a result, this triangular molecule is claimed to be less unstable than perhaps expected. The cyclobutane molecule, however, is destabilized both by the walks of length 4 and also those of length 8. Dewar would term this species σ antiaromatic.

Zimmerman[15b] has neatly shown how, for example, it is the presence of a Hückel 4-ring at the transition-state geometry which makes the disrotatory ring closure of butadienes unfavorable. Correspondingly it is the presence of a Möbius 4-ring at the transition-state geometry which makes the disrotatory route favored.

Clearly there are two effects to consider in viewing the stability of rings of various sizes. The first is that the bond angles at each center change with ring size. As the angle moves away from the ideal tetrahedral value, then the energy increases. This would be called angle strain. The second is the one we have emphasized in these papers, namely the energetic effect associated simply with the connectivity of the system and the generation of orbital loops of various sizes.

It is easiest to see the relative importance of the two effects by examining the case of the 4-ring. As we show later bond angle changes induce a change in the fourth (and higher) moments. The electronic effect of constructing the 4-ring itself also occurs at the fourth moment and so the two are directly comparable. Extracting the relevant figures from Table II we have

	108° chain	90° chain	4-ring
μ_4	6.041	6.789	7.706

This indicates that the angle strain and the effect of forming the ring make contributions to μ_4 of the same order of magnitude. The latter, however, is more important. Both effects work to increase μ_4, which at $X = 0.5$ represents a destabilizing contribution to the energy. For the 3-ring, Table II shows a large contribution to μ_3. Clearly there is a very strong energetic effect here on forming the ring. There is also a large change in μ_4 as

(14) See, for example: Eliel, E. L. "Elements of Stereochemistry"; Wiley: New York, 1969.

(15) (a) Dewar, M. J. S. *Bull. Chim. Soc. Belg.* **1979**, *88*, 957. (b) Zimmerman, H. E. *Acc. Chem. Res.* **1971**, *4*, 272.

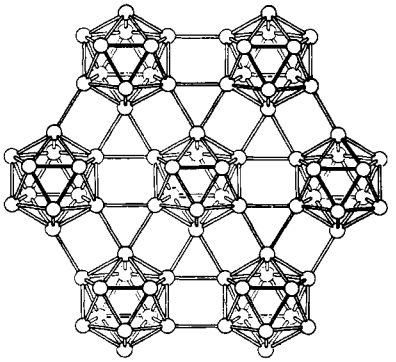

Figure 9. One sheet of the icosohedra of which rhombohedral boron is composed. The sheets themselves are stacked so as to form a cubic close-packed network of icosohedra.

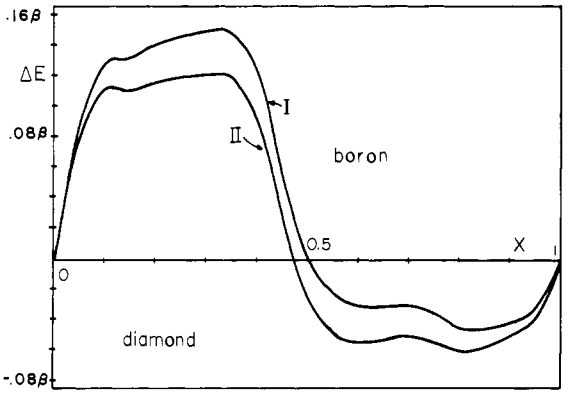

Figure 10. Difference in energy of stabilization by band filling between rhombohedral boron and cubic diamond. The convention is that when the curve is above the line, rhombohedral boron is the more stable, and when below the line, diamond is the more stable. I represents the curve where rhombohedral boron has been placed at the same density as diamond. In it, the shortest carbon–carbon distance is 1.57 Å. For II, the shortest carbon–carbon distance has been set at 1.59 Å. See Appendix section II for details of the calculation. The calculation uses the first 25 moments.

a result of the angle change. Here again both effects are important. However, since the ring-forming effect occurs in the third moment but the angle strain in the fourth moment, it is difficult to energetically weight the two effects.

Given that 3-rings are stabilized strongly at electron counts less than the half-filled band, it is clear that in general we expect the group 13 structures of Table IV to be stabilized at this point in the periodic table. The boron structures for example are typified by the packing together of icosahedra—polyhedra which contain a multitude of 3-rings (see Figure 9 for example). There is, however, a problem using one-electron models such as ours to quantify the relationships between the structures of the two groups. The coordination numbers in the two sets of structures are very different. In terms of the moments approach, systems with different coordination numbers will contain an energetic difference determined by the second moment differences. For example, consider two species A and B with coordination numbers V_A and V_B, respectively. Let us assume that the interatomic interaction integrals are equal in both systems. Then

$$\mu_2^A = V_A\beta^2 \qquad \mu_2^B = V_B\beta^2$$

(This in fact is a result well-known from graph theory.[16]) Then

$$\mu_2(\Delta\rho) = (V_A - V_B)\beta^2 \qquad (4)$$

By using the ideas of the previous paper in this issue, we expect our energy difference curve between A and B of the form of Figure 1a (top), where the system with the higher coordination number is stabilized at all X. This result, invariably not true in practice, is a problem associated with one-electron models in general and we should exercise caution when comparing energetically systems with different values of μ_2. Figure 10 shows a calculated energy difference curve for the rhombohedral boron (Figure 9) and cubic diamond (Figure 5). The presence of 3-rings manages to a large extent to overcome the discrepancy in μ_2 (shown in Table VI), and the energy difference curve is similar to that expected from Figure 1. Two curves are shown. One, using a constant density approximation, produces a node at the half-filled point. The other, using more realistic interatomic distances, shows in fact diamond to be stable at four electrons/atom and rhombohedral boron to be stable at three electrons/atom.

One other structure in Table IV is noteworthy in this section. We have commented on the structure of white tin before[17] and regarded it as derived from the simple cubic structure by breaking alternate linkages in two dimensions. In this way it is interesting to see that, using the language of the present work, the energetic destabilization of the 4-rings at the half-filled point is relieved on distortion away from simple cubic. We will discuss this effect later in the paper.

It is interesting to note at this point the prevalence of 3-rings in "electron-deficient" molecules—typified by the boranes, carboranes, and transition-metal cluster compounds.[18] In molecular carbon chemistry, 3-rings are seldom found but they are certainly a feature of boron and metal cluster chemistry. **8** shows three skeletons which contain five "heavy atoms". With a total of six

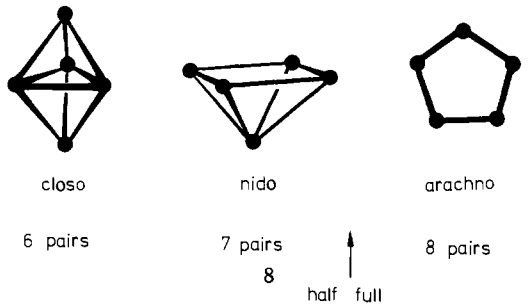

skeletal electron pairs, Wade's rules[19] predict a closo trigonal bipyramid (found for example for $C_2B_3H_5$) with many 3-rings. With seven skeletal electron pairs a nido octahedron is predicted. This geometry is found for B_5H_9 and probably for $C_5Me_5^+$. With eight skeletal electron pairs, an arachno pentagonal bipyramid is predicted, a structure found for $C_5H_5^-$. $X = 0.5$ occurs for a

Table VI. Boron R-12 vs. Diamond Structure[a]

	diamond	boron R-12
μ_2	1.0000	1.2544 (1.0000)
μ_3	−0.4729	−1.6540 (−1.1773)
μ_4	2.5842	6.2097 (3.9466)
μ_5	−2.8458	−16.7936 (−9.5299)
μ_6	9.6623	55.4005 (28.0701)

[a] The above calculations were done at the true diamond density, using carbon parameters throughout. Only first nearest-neighbor interactions were considered. In parentheses we give boron R-12 moments in standard form.

Table VII. Observed Main Group Fifth-Row Element Structures

	Tl	Pb	Bi	Po
configuration	s^2p^1	s^2p^2	s^2p^3	s^2p^4
X (p band)	0.167	0.33	0.50	0.67
structure	hcp	fcc	α-Bi	simple cubic
dominant ring	3	3	6	4

(16) See, for example: Hoffman, A. J. In "Studies in Graph Theory"; Fulkerson, D. R., Ed.; Mathematical Society of America; New York, 1975; Vol. 12, Part II.

(17) Burdett, J. K.; Lee, S. *J. Am. Chem. Soc.* **1983**, *105*, 1079.

(18) For example: Johnson, B. F. G., Ed. "Transition Metal Cluster Compounds"; Wiley: New York, 1979.

(19) See, for example: Wade, K. *Adv. Inorg. Chem. Radiochem.* **1976**, *18*, 1.

Table VIII. Moments for Fifth-Row Elemental Structures[a]

	α-Bi	α-Po	fcc	hcp
μ_2	1.0000	0.9933 (1.0000)	0.9230 (1.0000)	0.9230 (1.0000)
μ_3	0	0	−0.4906 (−0.5532)	−0.4906 (−0.5532)
μ_4	1.6407	1.7976 (1.8217)	1.5850 (1.8604)	1.5957 (1.8730)
μ_5	0	0	−1.7116 (−2.0912)	−1.7387 (−2.1242)
μ_6	3.2876	4.1169 (4.2003)	3.7128 (4.7215)	3.7344 (4.7490)
μ_7	0	0	−5.4745 (−7.2464)	−5.5016 (−7.2823)
μ_8			10.6372 (14.6555)	13.6378 (14.4654)

[a] The above moments are for first nearest-neighbor σ-only interactions for α-Po, fcc, and hcp. They include second nearest-neighbor α-Bi interactions. Calculations were performed with Bi parameters with all densities set equal to the true α-Bi density. Moments in standard form are given in parentheses.

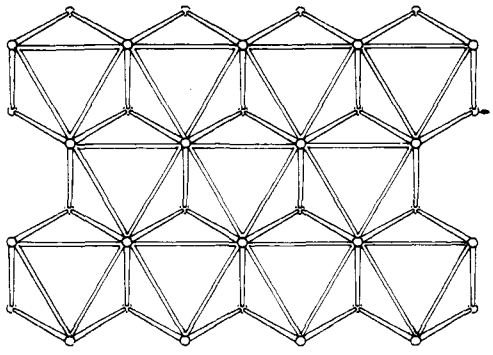

Figure 11. Two layers of a close packing. For a fuller description of the fcc and hcp structures, see Appendix section I.

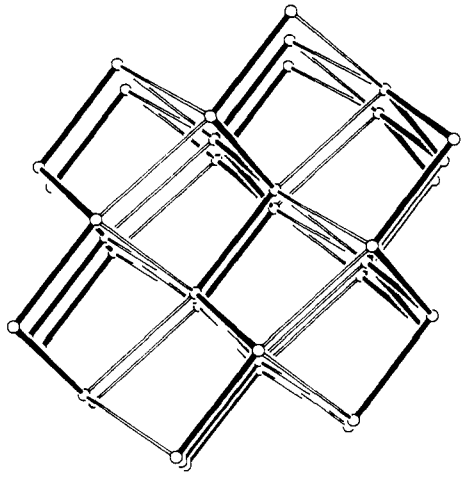

Figure 12. α-Bi structure. In this drawing the relation of it to the simple cubic structure has been emphasized. See **44** for a clear picture of its three-coordinate sheets.

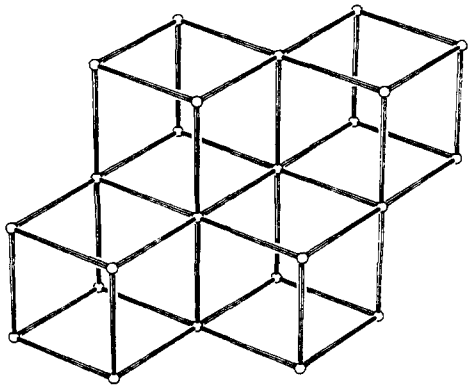

Figure 13. Simple cubic structure.

skeletal electron count of $7^1/_2$ pairs. Notice how the 5-ring is found just after the half-filled point (see Figure 1). Although in this paper we shall make several comparisons between molecules and solids, because of the frequent coordination number differences of the atoms in a molecule (for example the nido octahedron of **8** which contains three- and four-coordinate atoms), the qualitative ideas associated with the curves of Figure 1 may not be as reliable. (See the previous paper[2] in this issue for a discussion of the effect of coordination number variations.) In addition the discrete nature of the molecular eigenvalue spectrum may also produce some local distortions in the $\Delta E_n(X)$ curves.

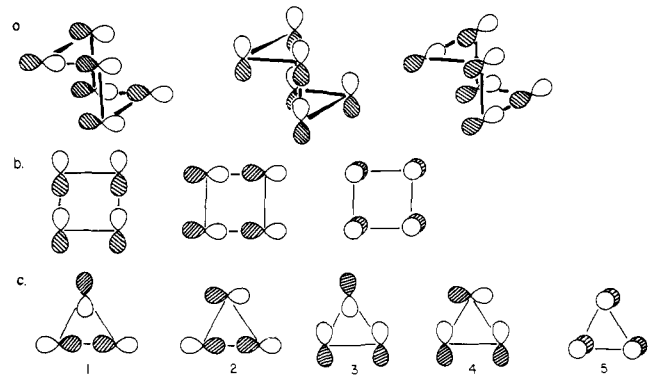

Figure 14. (a), (b), and (c) The principal rings present in the α-Bi, simple cubic, and close packing structures, respectively. In (a) we have for the sake of convenience set bond angles at 90° (in the calculations as in the crystal structure itself, the bond angles are set at 95°). It can be seen that only the three illustrated paths are allowed. All three are Hückel paths. In (b) again it is found that all paths are Hückel. Only in (c) is there seen to be one Möbius path (which is labeled 2). Clearly the net effect of the five paths shown in (c) is a Hückel one.

IV. Heavy Main Group Elements

The chemistry of Tl, Pb, Bi, and Po is distinguished from that of lighter main group elements by the presence of an inert pair of electrons. Thus, Tl^I and Pb^{II} are common oxidation states for these heavy elements while B^I and C^{II} are not. The inert pair of electrons in these species is the $6s^2$ pair, and the orbital contraction required to make them corelike probably arises through relativistic effects.[20] As a result we may exclude the 6s electrons from consideration and concentrate on the effect of the p orbitals in these structures. The most stable structures for these elements[13] are shown in Table VII along with the dominant ring present. The structures themselves are depicted in Figures 11–13. It is not hard to see that for each of these rings, their net effect is of a Hückel and not Möbius type. This is shown in detail in Figure 14.

We may therefore immediately apply the rules developed earlier to understand the stability of these ring systems. Below the half-filled band we anticipate the stability of three-membered ring structures (fcc and hcp), at the half-filled point the stability of six-membered ring structures (α-bismuth), and near the full band four-membered ring structures (simple cubic). As in the previous section, we must be careful in dealing with the very different coordination environments in these systems in any calculations.

(20) (a) Pitzer, K. S. *Acct. Chem. Res.* **1979**, *12*, 271. (b) Pykko, P.; Desclaux, J.-P. *Acct. Chem. Res.* **1979**, *12*, 276.

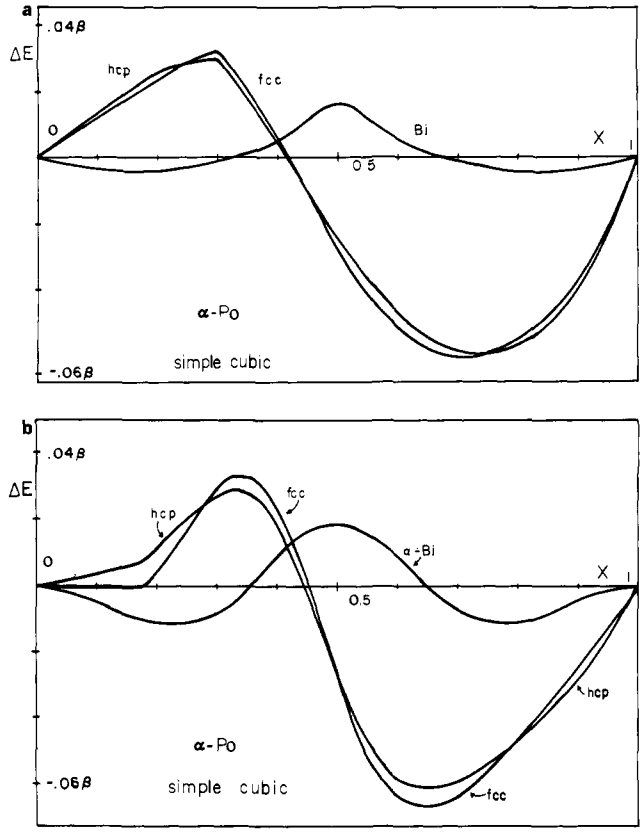

Figure 15. Difference in energy of stabilization by band filling for the fifth-row structure types. See caption of Figure 3 for conventions used (here the role of graphite has been replaced by simple cubic): (a) second-order Q polynomial approximation,[2] (b) equivalent of a full band calculation using the continued fraction method using the first 30 moments.[2] See Appendix section II for details of the calculation.

There is no difficulty in comparing hcp to fcc—the coordination in the former is a truncated trigonal prism and in the latter a cuboctahedron, two 12-coordinate environments. Furthermore, by analogy with elemental antimony, which under pressure transforms to the simple cubic structure with almost no change in density, we may fix the densities of the α-bismuth and simple cubic structures to be equal. Unfortunately there is no firm information available which adjoins hcp and fcc to the other two structures. Our results, shown in Figure 15 and Table VIII, have been derived from calculations where equal densities were chosen for all four structures. At $(6p)^1$, hcp is most stable, at $(6p)^2$ fcc, and at $(6p)^3$ α-bismuth, and at $(6p)^4$ we find the α-bismuth to simple cubic crossing point. The results are in quite nice agreement with experiment.

In Appendix section I we discuss the structural factors which determine the energy difference between fcc and hcp arrangements. To summarize the results given there, the form of the energy difference curve is determined by the different conformations of the five-membered rings in the two structures. As a result, densities of states of the two structures differ at the fifth moment. The energy difference curve we expect to see will look something like that shown in **9**, which suggests that the fcc

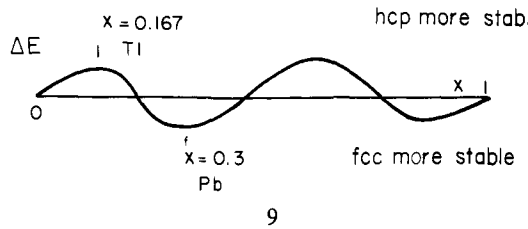

9

structure should be more stable for Pb but hcp more stable for Tl. This result is in accord with the plots of Figure 15.

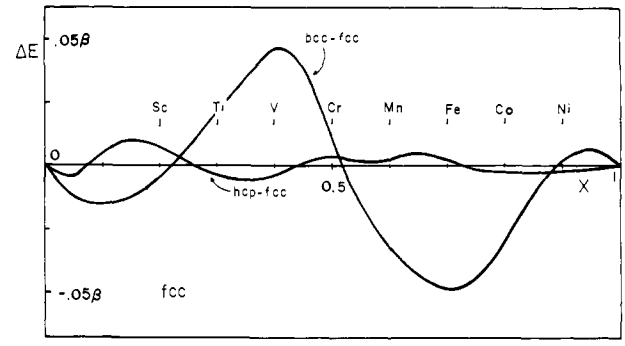

Figure 16. Difference in energy of stabilization by band filling for transition-metal structures. See caption of Figure 3 for conventions used. Calculation used the first 30 moments. (See Appendix section II for details.)

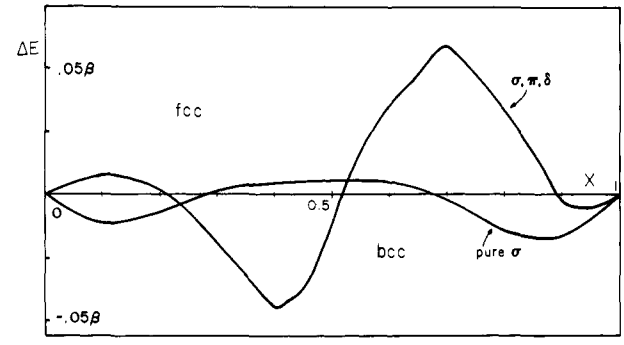

Figure 17. Comparison between the σ-only model and the full σ, π, and δ model for transition metals. Conventions are the same as those described in the caption of Figure 10. Calculations involve the first 30 moments.

V. Transition Elements

The ability of Hückel theory to broadly differentiate between nonmagnetic structural types for these elements is well-known.[21,22] Figure 16 shows the result of a calculation of this type which shows a good correlation with the observed structure types of Table IX if it is assumed that the electronic configuration of the metal is represented as s^1d^{n-1}. The trend hcp–bcc–hcp–fcc as the table is traversed is correctly reproduced but there are some errors in an absolute sense. The prediction for the d^3 metal is in error and all Hückel calculations of this type show an erroneous stability field for the bcc structure at high band fillings.

The moments method was applied to the problem of transition-metal structures by Cyrot-Lackmann[23] who recorded the first few moments of these three basic structures and also studied stacking problems and surface tension properties. Experience in the area of molecular transition-metal chemistry suggests that a σ-only model of metal–metal interaction might be a useful starting point for these elemental structures. We may write the interatomic overlap integrals[24] (which determine the interaction integrals) as simple decomposition into σ, π, and δ components

$$S = \sum_{\lambda=\sigma,\pi,\delta} S_\lambda f(\lambda,\theta,\varphi) \qquad (5)$$

where the two orbitals concerned are related via the polar coordinates θ and φ. (S_λ itself, of course, depends upon the interatomic distance and the radial part of the atomic wave function.) The

(21) (a) Pettifor, D. G. *Calphad: Comput. Coupling Phase Diagrams Thermochem.* **1977**, *1*, 305. (b) Pettifor, D. G. *J. Phys. C* **1970**, *2*, 366. (c) Duthie, J.; Pettifor, D. G. *Phys. Rev. Lett.* **1977**, *38*, 564.

(22) Burdett, J. K. *J. Phys. Chem.* **1983**, *87*, 4368.

(23) (a) Cyrot-Lackmann, F. *J. Phys. Chem. Solids* **1968**, *29*, 1235. (b) Ducastelle, F.; Cyrot-Lackmann, F. *J. Phys. Chem. Solids* **1970**, *31*, 1295; **1971**, *32*, 285.

(24) See, for example: Burdett, J. K. "Molecular Shapes"; Wiley: New York, 1980.

Table IX. Observed Transition-Metal Structures[a]

3	4	5	6	7	8	9	10	11
Sc	Ti	V	Cr	Mn	Fe	Co	Ni	Cu
hcp	hcp	bcc	bcc	α-Mn[b,c]	bcc[c]	hcp[c]	fcc[c]	fcc
fcc			hcp					
Y	Zr	Nb	Mo	Tc	Ru	Rh	Pd	Ag
hcp	hcp	bcc	bcc	hcp	hcp	fcc	fcc	fcc
La	Hf	Ta	W	Re	Os	Ir	Pt	Au
abac[d]	hcp	bcc	bcc	hcp	hcp	fcc	fcc	fcc

[a] Low-temperature and -pressure forms. [b] See ref 13 for details of structure. [c] Magnetic at room temperature. [d] abac close packing is a structure intermediate between hcp and fcc.

Table X. Transition-Metal Elemental Structures

	fcc (σ, π, and δ)	bcc (σ, π, and δ)	hcp (σ, π, and δ)
μ_2	1.0000	1.0067 (1.0000)	1.0000
μ_3	−0.2495	−0.2971 (−0.2942)	−0.2495
μ_3	1.8553	1.7488 (1.7257)	1.8357
μ_5	−1.2688	−1.2136 (−1.1936)	−1.2217
μ_6	4.7233	4.3826 (4.2960)	4.4617
μ_7	−5.6320	−5.2588 (−5.1377)	−4.9948
μ_8	15.3103	15.0553 (14.6597)	13.3024
	fcc (σ only)	bcc (σ only)	
μ_2	0.5346 (1.0000)	0.5317 (1.0000)	
μ_3	−0.0020 (−0.0050)	0	
μ_4	0.5250 (1.8372)	0.5541 (1.9603)	
μ_5	−0.0025 (−0.0118)	0	
μ_6	0.6414 (4.1980)	0.7175 (4.7746)	
μ_7	−0.0035 (−0.0317)	0	
μ_8	0.8943 (10.9493)	1.0333 (12.9331)	
	simple cubic first and second nearest neighbors	simple cubic first nearest neighbors only	
μ_2	1.2703 (1.0000)	1.1853 (1.0000)	
μ_3	−0.3539 (−0.2472)	0	
μ_4	3.7065 (2.2971)	3.0009 (2.1360)	
μ_5	−2.6724 (−1.2217)	0	
μ_6	15.5994 (4.4617)	9.5246 (5.7198)	
μ_7	−18.9660 (−4.9948)	0	
μ_8	82.1308 (13.3024)	33.9406 (17.1959)	

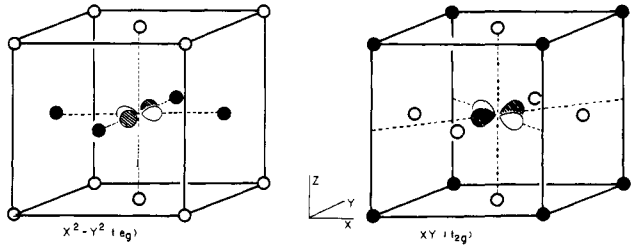

Figure 18. Overlap between d orbital neighbors in the bcc structure. Circles represent atoms which belong to the coordination sphere of a lattice site. For the sake of visual clarity, second nearest neighbors have been moved in closer so that they lie in the center of the faces of the cube, while first nearest neighbors are accurately portrayed at the corners of the cube. Empty circles represent atoms which lie on a σ nodal plane. Filled circles do not lie on a σ nodal plane. The $x^2 - y^2$ and xy orbitals are taken as representatives of the e_g and t_{2g} sets, respectively. It can be seen that in the case of e_g orbitals, there is no σ overlap with first nearest neighbors, and in the case of t_{2g} orbitals, there is no overlap with second nearest neighbors.

σ-only model entails setting $S_\pi = S_\delta = 0$ in eq 5. The resulting energy difference curve is shown in Figure 17 and shows a dramatically different result when compared to that of Figure 16. In particular, note the opposite predictions for the group 5 and 6 elements. π bonding is then an important effect in determining elemental transition-metal crystal structure. In fact S_π is approximately one-half to three-fourths the size of S_σ. This shows up very noticeably in the moments of Table X. Also important are the second nearest neighbors in the bcc structure, only 14% further away than the nearest neighbors.

One very striking feature of the pure σ DOS for fcc and bcc (and hcp) is their near or total symmetry around $E = 0$. As Table X shows, this is due to the identically zero values of the odd moments in the bcc structure and the very small values in the close-packed structures. The reasons for this are straight-forward. While all three structures contain odd loops, their weight is determined by the overlap of the orbitals involved. In the case of the σ-only model, many of these are either zero or small. Figure

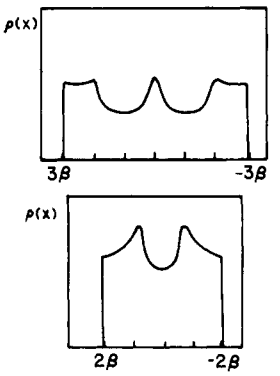

Figure 19. DOS of (top) t_{2g} and (bottom) e_g d orbitals in the bcc σ-only model.

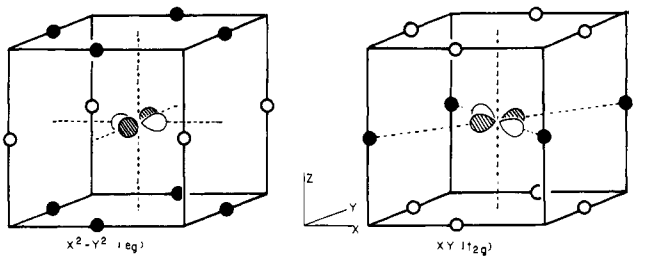

Figure 20. Overlap between d orbital neighbors in the fcc structure. For conventions see caption of Figure 18. The almost bipartite character of the σ-only model in fcc can be anticipated in part by noting that four of the five orbitals (including the two shown here) when considered singly *are* bipartite.

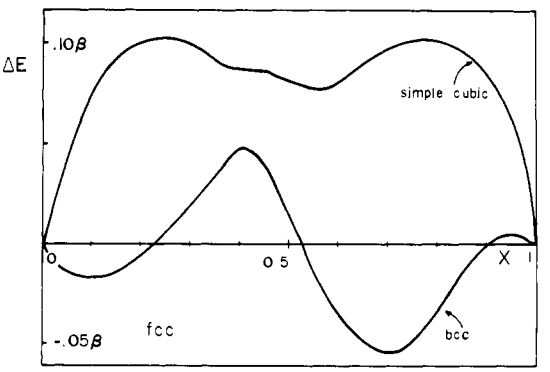

Figure 21. Difference in energy of stabilization between the simple cubic and fcc structures for the transition metals. The calculation is based on the first 25 moments. Note how the simple cubic/fcc curve (dominated in qualitative terms by μ_2) as a strong μ_4 modulation. For comparative purposes the fcc–bcc curve is also included.

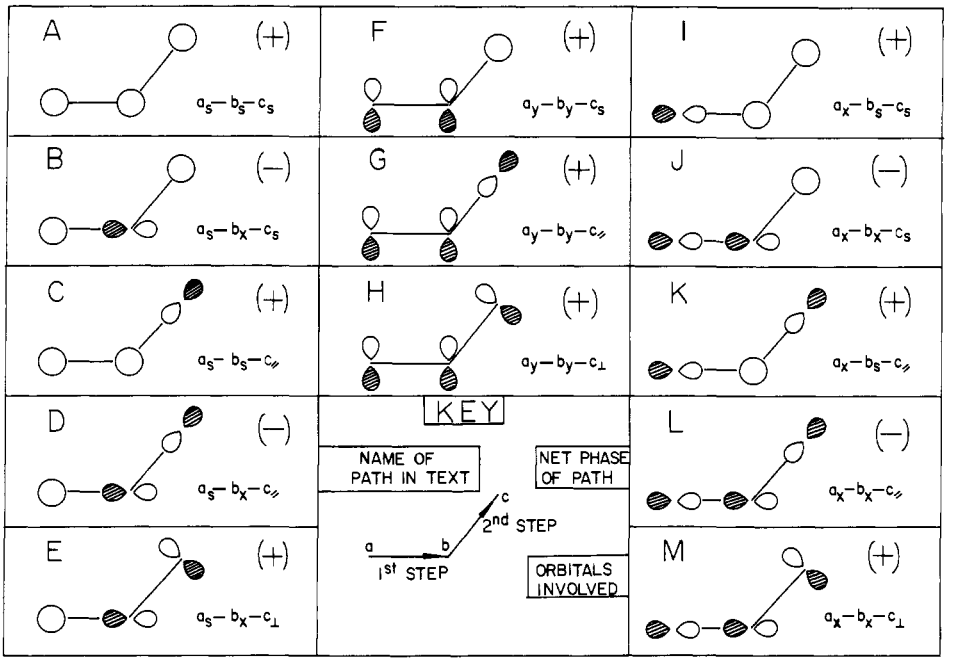

Figure 22. Enumeration of all steps of length 2 which feel the effect of bond angle alternation. Letters are referred to in the text. The net phase shown indicates whether the half path is Hückel (+) or Möbius (−).

18 shows how, for the bcc structure, all first nearest neighbors lie on the σ nodal plane of the t_{2g} orbitals. All $\langle t_{2g}|e_g\rangle$ overlap integrals then vanish. As a result, all the odd moments for such a structure are zero, since, for a walk to be odd in length, it must in its path contain steps to first and second nearest neighbors. Any such path must involve a jump from an e_g to t_{2g} orbital, a path of zero weight. Within the σ-only model, the striking result is that the d orbitals form two separate bipartite networks. Those of t_{2g} symmetry involve interactions with the first nearest neighbors only and those of e_g symmetry with the second nearest neighbors only. The densities of states for the two orbital sets on this model show perfect symmetry about $E = 0$ (Figure 19).

For the fcc structure, with 12 equidistant neighbors, the geometrical relationship shown in Figure 20 is sufficient to show that some at least of the integrals, zero in bcc, will be nonzero in this structure. In particular the pair of orbitals shown in **10**, orthogonal in bcc, are not so in the fcc structure. Examination of this problem

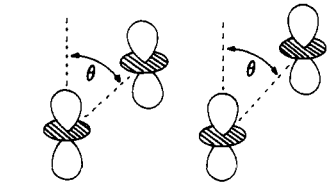

$f(\sigma,\theta,\phi) = 0$ bcc $\theta = 54.73°$ $\quad$ $f(\sigma,\theta,\phi) = 0$ fcc $\theta = 45°$

10

in a little more detail shows that when the σ-only model is used, it is impossible to construct a three-step closed walk which involves any t_{2g} orbital. Similarly there are few such walks which involve purely e_g orbitals, and these are weighted by small overlap integrals (**10**). Therefore, μ_3 is near zero. As a consequence of these structural features, the difference in energy between fcc and bcc structures using this model is dominated by the even moments. Examination of Table X shows that the fourth moment is dominant and the energy difference curve in Figure 17 has the shape expected.

A knowledge of the first four different moments for the three structures allows construction of $\Delta E(X)$ curves in good agreement with the ones of Figures 16 and 17. This corresponds to the second-order Q approximation of the previous paper in this issue. Interestingly, if the eighth moment differences are ignored, the correct structure (fcc) is predicted at the right-hand side of the plot of Figure 16. The bcc stability field at high X has disappeared. Otherwise the energy difference plot is similar to the one generated by inclusion of the eighth moment.

In comparing these structures, we have followed earlier workers[23] and compared these structures at constant density. As we suggested earlier this is not always the most realistic approach. In Figure 21 (and in Table X) can be seen the relative stability of the simple cubic structure when compared to its rivals. Here μ_2 is so large for the simple cubic arrangement (each atom is six-coordinate, but now the interatomic distances are very short) that it is predicted to be the most stable structure at all X (see Figure 1). Notice the ripples of higher moment differences superimposed upon an overwhelmingly dominant second moment difference curve. This highlights once more the inadequacy of one-electron models in differentiating structures where bond length and/or coordination number differences are large.

VI. Angle Changes

Bond angle changes play a substantial role in Hückel energetics. Indeed in the absence of three- and four-membered rings, such effects may well be the dominant features of energy difference curves as we mentioned in section II above. **11** and **12** illustrate the two lowest order walks which can support bond angle effects.

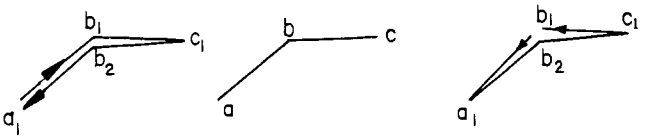

11 12

11 shows a walk which will contribute to the DOS of orbital a_1 located on atom a. It is a path which starts at orbital a_1 and hops to orbitals b_1, c_1, and b_2 in that order before returning to orbital a_1. This may be written more compactly by using a notation similar to that used in permutation cycles as $[a_1b_1c_1b_2]_{a_1}$ where the subindex of the entire cycle a_1 denotes the starting orbital. **12** is therefore $[b_1a_1b_2c_1]_{b_1}$. The double index used here allows

Table XI. μ_4 Dependence on Bond Angle

	90° [b]	120°	180°
	a. μ_4 for Triatomic Molecule[a]		
C	1.0	0.90	0.81
As	1.0	0.90	0.91
Bi[c]	1.0	1.21	1.85
	b. μ_4 for Infinite Chain		
C	1.0	0.83	0.70
Te	1.0		0.90
	c. μ_4 for Puckered Graphite Sheet		
C	1.0	0.76	
Te	1.0	0.80	

[a] We consider μ_4 of the singly coordinate atom here. [b] μ_4 of the 90° conformation has been normalized to one for all structures. Angle refers to the angle between the bonds. [c] Bi calculation is based on a p orbital only model.

us to specify the atom (a,b,c,...) and the orbital (1,2,...) on that atom. Specifically we will use such a notation to represent the weight of such a walk, important in evaluating the relevant moment of the energy spectrum.

$$[a_1b_1c_1b_2]_{a_1} = H_{a_1b_1}H_{b_1c_1}H_{c_1b_2}H_{b_2a_1} \quad (6)$$

With such a notation it is clear that

$$[a_1b_1c_1b_2]_{a_1} = [b_1a_1b_2c_1]_{b_1} \quad (7)$$

The extra label outside of the bracket may be dropped when convenient, since the interaction integral product is independent of where the walk actually starts. Also the notation is a useful one since it allows us to decompose any given moment into its component parts. For example

$$\mu_4(\text{DOS of } a_1) = \sum_{rstv}\sum_{ijkl}[r_is_jt_kv_l]_{a_1} \quad (8)$$

where r,s,t,v and i,j,k,l are atomic and orbital indexes, respectively. In determining the moments of a given order, we shall follow the natural approach of first determining which paths are important and then weighting them by functions (the interaction integrals) proportional to overlap and finally summing over all the various atomic contributions. As an example, we see the equivalence between all the walks shown in **11** and **12** since

$$\sum_{i,j,k,l}[a_ib_jc_kb_l] = \sum_{i,j,k,l}[b_ic_jb_ka_l] \quad (9)$$

In studying the effect bond angles have on μ_4, we need only examine paths of the type shown in **11**. We now examine some specific examples.

p Orbitals Only. Here each atom is populated with three p orbitals, and the Hückel α is set equal to 0. The three sets of orbitals are shown in **13**, and we need to study the effect on μ_4 of variations in the angle φ. Accordingly we will ignore any

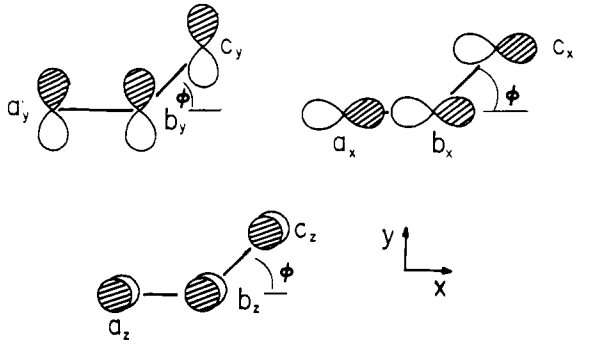

13

φ-independent components of μ_4. We may therefore ignore (a) any walk of length 4 which involves p_z orbitals (any walk which involves a p_z orbital must be exclusively associated with such orbitals, since they are of opposite parity (with respect to the molecular plane) to the p_x and p_y orbitals; such p_z–p_z interactions are angle independent) and (b) any walk of length 4 which involves orbitals on only two atoms.

Table XII. μ_5 Bond Angle Effects

path	μ_4 contribution	conversion factor to μ_5 contribution	μ_5 contribution
	a. $\mu_4(a_x)$ and $\mu_5(a_x)$ for φ = 0° [a]		
$[a_xb_xc_xb_s]$ & $[a_xb_sc_xb_x]$	$-\beta^4$	$^1/_3\alpha$	$-^1/_3\alpha\beta^4$
$[a_xb_xc_sb_x]$	$^1/_2\beta^4$	$^1/_3\alpha$	$^1/_6\alpha\beta^4$
$[a_xb_sc_sb_x]$ and $[a_xb_xc_sb_s]$	$-^1/_2\beta^4$	$-\alpha$	$^1/_2\alpha\beta^4$
$[a_xb_sc_xb_s]$	$^1/_4\beta^4$	$-\alpha$	$-^1/_4\alpha\beta^4$
$[a_xb_sc_sb_s]$	$^1/_8\beta^4$	$-2^1/_3\alpha$	$-^7/_{24}\alpha\beta^4$
$[a_xb_xc_xb_x]$	β^4	$^5/_3\alpha$	$^5/_3\alpha\beta^4$
total	$^3/_8\beta^4$		$^4/_3\alpha\beta^4$
	b. $\mu_4(a_x)$ and $\mu_5(a_x)$ for φ = 90° [a]		
$[a_xb_sc_yb_s]$	$^1/_4\beta^4$	$-\alpha$	$-\alpha\beta^4$
$[a_xb_sc_sb_s]$	$^1/_8\beta^4$	$-2^1/_3\alpha$	$-^7/_{24}\alpha\beta^4$
total	$^3/_8\beta^4$		$-1^7/_{24}\alpha\beta^4$
	c. $\mu_4(a_s)$ and $\mu_5(a_s)$ for φ = 0° [a]		
$[a_sb_sc_sb_s]$	$^1/_{16}\beta^4$	-5α	$-^5/_{16}\alpha\beta^4$
$[a_sb_sc_xb_s]$	$^1/_8\beta^4$	$-3^2/_3\alpha$	$-^{11}/_{24}\alpha\beta^4$
$[a_sb_xc_sb_s]$ and $[a_sb_sc_sb_x]$	$-^1/_4\beta^4$	$-3^2/_3\alpha$	$^{22}/_{24}\alpha\beta^4$
$[a_sb_xc_sb_x]$	$^1/_4\beta^4$	$-2^1/_3\alpha$	$-^7/_{12}\alpha\beta^4$
$[a_sb_xc_xb_s]$ and $[a_sb_sc_xb_x]$	$-^1/_2\beta^4$	$-2^1/_3\alpha$	$1^1/_6\alpha\beta^4$
$[a_sb_xc_xb_x]$	$^1/_2\beta^4$	$-\alpha$	$-^1/_2\alpha\beta^4$
total	$^3/_{16}\beta^4$		$0.229\alpha\beta^4$
	d. $\mu_4(a_s)$ and $\mu_5(a_s)$ for φ = 90° [a]		
$[a_sb_sc_sb_s]$	$^1/_{16}\beta^4$	-5α	$-^5/_{16}\alpha\beta^4$
$[a_sb_sc_yb_s]$	$^1/_8\beta^4$	$-3^2/_3\alpha$	$-^{11}/_{24}\alpha\beta^4$
total	$^3/_{16}\beta^4$		$-0.771\alpha\beta^4$

[a] See beginning of section on angle changes to interpret path symbols. Paths in this table refer to **11**, and φ is illustrated in **11** as well.

As a result, only four types of walk need to be considered (**14**–**17**). Referring to the angle-dependent part of μ_4 as μ_4', we

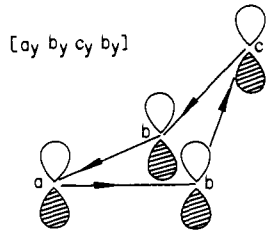

14

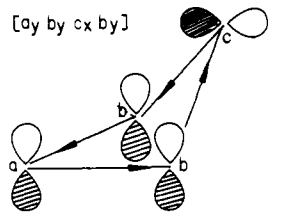

15

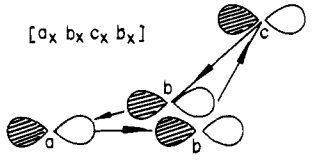

16

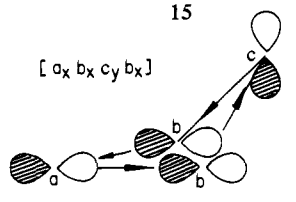

17

may simply write

$$\mu_4'(a_x) = \mu_4'(b_x) = 2\{[a_xb_xc_xb_x] + [a_xb_xc_yb_x]\} \quad (10)$$

$$\mu_4'(a_y) = \mu_4'(b_y) = 2\{[a_yb_yc_yb_y] + [a_yb_yc_xb_y]\} \quad (11)$$

Writing the interaction integrals as directly proportional to overlap (via a constant K) and recalling the angular dependence of these integrals, in terms of eq 5 (here of course $S_\delta \equiv 0$), then

$$\mu_4'(a_x) = KS_\sigma^2[\cos^2\varphi S_\sigma^2 + \sin^2\varphi S_\pi^2] \quad (12)$$

$$\mu_4'(a_y) = KS_\pi^2[\cos^2\varphi S_\pi^2 + \sin^2\varphi S_\sigma^2] \quad (13)$$

and

$$\mu_4'(a_x + a_y) = K[(S_\pi^4 + S_\sigma^4)\cos^2\varphi + 2S_\pi^2S_\sigma^2\sin^2\varphi] \quad (14)$$

Table XIII. Te and Se Chains

	moments (in standard form)					
	90° Te chain	180° Te chain	"tetrahedral" Te	α-Te	"tetragonal" Se	α-Se
μ_2	1.0000	1.0000	1.0000	1.0000	1.0000	1.0000
μ_3	-0.4266	-0.4266	-0.4588	-0.4588	-0.5445	-0.5445
μ_4	2.4957	2.2554	2.1135	2.1351	2.2156	2.3569
μ_5	-2.3918	-1.2608	-1.8262	-2.1893	-2.0365	-2.7005
μ_6	7.7989	5.4796	5.9634	5.7868	5.7868	7.1915
μ_7	-10.7593	-3.4279	-6.3863	-8.6534	-6.7756	-11.2478

Table XIV. C_x Chain

	90° chain	120° chain	180° chain
μ_2	1.0000	1.0000	1.0000
μ_3	-0.6003	-0.6003	-0.6003
μ_4	3.4541	2.8630	2.4019
μ_5	-4.1962	-3.5846	-3.0401
μ_6	15.2513	10.7726	7.7510
μ_7	-25.2429	-18.1464	-12.9919

Since $S_\sigma > S_\pi$ is always true we conclude that (a) $\mu_4(p_x)$ is greatest when $\varphi = 0°$, (b) $\mu_4(p_y)$ is greatest when $\varphi = 90°$, and (c) $\mu_4(p_{tot})$ is greatest when $\varphi = 0°$.

s and p Orbitals. As s orbital interactions are bond angle independent, we might at first have expected their inclusion to have little effect on our conclusions above. However, we know from Walsh's rules[24] that sp hybridization plays a crucial role in controlling molecular geometry. We again first consider only paths of the type shown in **11**. For such paths the problem is simplified by the parallelism between the first two steps in which one must walk from atom a to c and then the last two steps in which one must walk back from c to a. We may therefore divide our walks of length 4 into two equivalent walks of length 2, or, conversely, to produce a walk of length 4, we need merely to fuse together two walks of length 2. Furthermore we only need adjoin those walks of length 2 (connecting atom a to atom c) to those walks of length 2 (connecting atom c to atom a) such that for each walk of length 2, the two c_i orbitals and the two a_j orbitals included are the same. (Otherwise of course the loop will not be closed.) This is shown graphically in Figure 22 where we have introduced the extra convention of $c_\parallel$ and $c_\perp$ orbitals.

When the products of the interaction integrals in any walk of length 2 are defined as in eq 15 for A, B, etc., of Figure 22

$$[A] = H_{a_s b_s} H_{b_s c_s}$$

$$[B] = H_{a_s b_x} H_{b_x c_s}, \text{ etc.} \quad (15)$$

Then

$$\mu_4'(a_s) = ([A] + [B])^2 + ([C] + [D])^2 + [E]^2 \quad (16)$$

$$\mu_4'(a_y) = [F]^2 + [G]^2 + [H]^2 \quad (17)$$

$$\mu_4'(a_x) = ([I] + [J])^2 + ([K] + [L])^2 + [M]^2 \quad (18)$$

In these equations lies the possibility of diffraction-type interference.[25] [A] and [B] are of opposite sign (see Figure 22) and will interfere with each other in the expression $([A] + [B])^2$. Similary there is the possibility of interference between [C] and [D], [I] and [J], and finally [K] and [L]. Such interference is always destructive as may be seen by inspection of the phases of the relevant expressions shown in Figure 22. This interference will dominate the variation in μ_4 if $|S_\sigma/S_\pi| \sim 1$ since, in such cases the pure p orbital interactions are insensitive to bond angle, as described above. To maximize μ_4, such interference needs to be minimized. We first note that of the four pairs of interfering walks, half are bond angle invariant (A, C, I, and K). If B, D, J, and L are generally of greater magnitude than A, C, I, and K, maximization of μ_4 requires maximizing the overlaps in B, D, J, and L. If the converse is true then, to maximize μ_4 we will need to minimize the overlaps in B, D, J, and L. Generally B, D, J, and L have smaller overlaps than their partners since, as a rule, $|S_{sp}| \sim |S_{pp}|$ and $|H_{ss}| > |H_{pp}|$, and so the relevant interaction integrals lie in the order, $|H_{ss}| > |H_{sp}| > |H_{pp}|$. [A], [C], [I], and [K] contain more s orbital contributions and so the overlaps in [B], [D], [J], and [L] must be minimized to maximize μ_4.

When interference is important we find μ_4 (p_{tot}) is greatest when φ is 90° and μ_4 (s_{tot}) is greatest when φ is 90° for all the walks of the type shown in **11**. These results are the exact opposite to the pure p orbital case, a result which will be important below.

Dependence on the Row of the Periodic Table. The actual behavior found for a given system will, as we have indicated above, be sensitive to the specific values of the interaction integrals between the orbitals on adjacent atoms. In first-row elemental structures s–p, s–s, and p–p(π) overlaps are good. The importance of π bonding for first-row elements is often used to rationalize the frequently different chemical behavior and structural patterns of these elements compared to their congeners. The atomic s–p separation is large. We therefore expect μ_4 to be greatest when the bond angles are 90° and smallest when 180°. In contrast, for the fifth-row elements, s–s, s–p, and p–p(π) overlaps are weak. To a good extent the s orbitals are inert and may be excluded from the valence set. We therefore expect μ_4 to be greatest when angles are 180°. In Table XI we compare the dependence of μ_4 on bond angle for various elements by using Slater orbitals and typical interatomic separations (see Appendix section II). Notice that the changes in μ_4 on bending are largest for the light (s and p orbitals) and heavy (p orbitals only) elements and smallest for those in between. The anticipated variation in the fourth moment is actually observed numerically, and we can see that at the half-filled band, the lighter elements should form structures with wide bond angles, while the isoelectronic heavy elements should form structures with much smaller angles.

Table XI also shows the dependence of μ_4 changes on coordination number. The overall effect which bond angles have on the fourth moment is greatest when the number of paths of type **11** and **12** is largest. We therefore expect μ_4 effects to be most important when considering the puckering of a graphite sheet and least important in the case of bending a triatomic molecule.

Importance of μ_5. The reversal in the sign of the changes in μ_4 on bending between first- and fifth-row elements implies that in between, the fourth moment may not be the dominating structural influence. We therefore turn our attention to the fifth moment. In the fifth moment, just as in the fourth, all angle-dependent paths must involve exactly three different atoms. Nevertheless, there can exist strong differences between the two moments. We illustrate this with the following example (based loosely on elemental tellurium).

Let $S_\pi(pp) = 0$ and let $-\beta, \beta/(2)^{1/2}$ and $-\beta/2$ be the maximum possible interaction integrals between two adjacent p orbitals, two adjacent p and s orbitals, and two adjacent s orbitals, respectively. Finally let $H_{ss} = -\alpha$ and $H_{pp} = \alpha/3$. This last condition just sets $\mu_1 = 0$. In Table XII we see that for this example, there is no μ_4 dependence upon bond angle (at least when comparing 90° to 180°). There is, though, a very strong μ_5 dependence on angle. This is readily seen to be due to the H_{pp} diagonal term which is positive and therefore has the effect of turning Hückel 4-walks into Möbius 5-walks. These Möbius 5-walks are important because in the linear case, $S_\sigma(pp)$ is large and therefore p orbital dominant paths make up a large portion of the total sum. **18** shows how

(25) See a related interference problem in: Edmiston, C.; Ruedenberg, K. *Rev. Mod. Phys.* **1963**, *35*, 457.

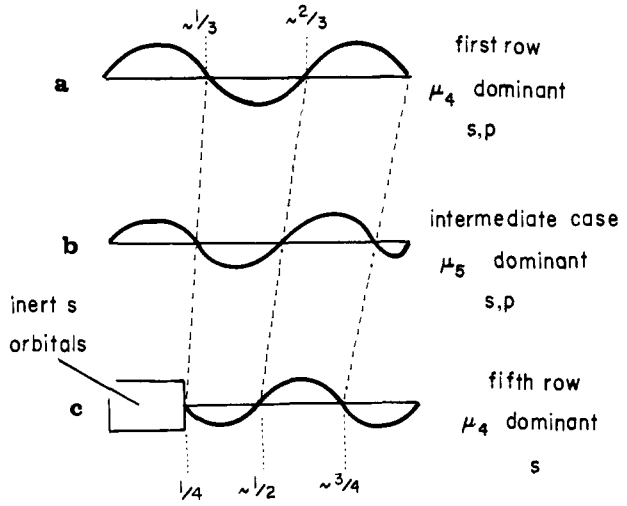

Figure 23. Qualitative changes which occur in ΔE, the energy difference between linear and bent geometries, on descending a main group column.

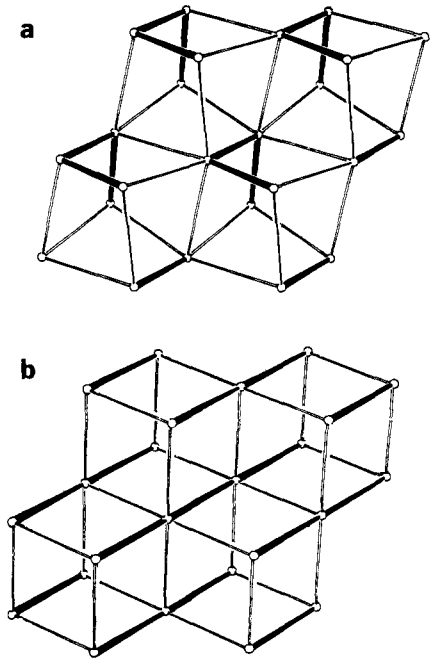

Figure 24. (a) α-Se and α-Te structures. (b) Tetragonal distortion mentioned in the text. Both have two short (dark lines) and four long (thin lines) bonds for each atom. Compare these structures to the simple cubic structure of Figure 13.

such an effect changes the $\Delta E(X)$ curve—an extra lobe appears at high X.

18

Of particular interest is the linking together of the predictions we have made in this section. Figure 23 shows the smooth transitions between the cases we have discussed. Of most striking interest is the movement of the changeover points from linear to bent structures on moving down the periodic table. Particularly note that at just above the half-filled point, the opposite results are found at the top and bottom of the table as are predictions for species close to the filled band.

Comparison with Experiment. In the area of extended solids there is a dearth of experimental data to compare with the predictions of Figure 23. The chalcogens form chain structures (with the exception of polonium). These are spiral arrangements where

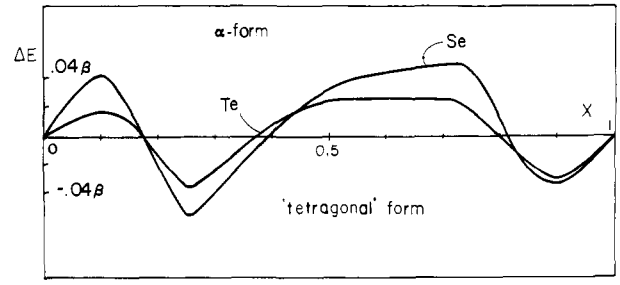

Figure 25. Difference in energy of stabilization by band filling for the α-Se and α-Te structures vs. the tetragonal distortions of Se and Te. Details of calculation are given in Appendix section II. The calculation is based on the first 30 moments.

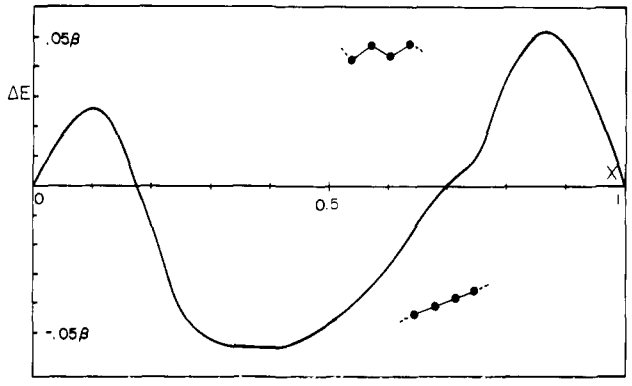

Figure 26. Difference in energy of stabilization by band filling for a bent vs. a linear carbon chain. Details of calculation are given in Appendix section II. The calculation is based on the first 30 moments.

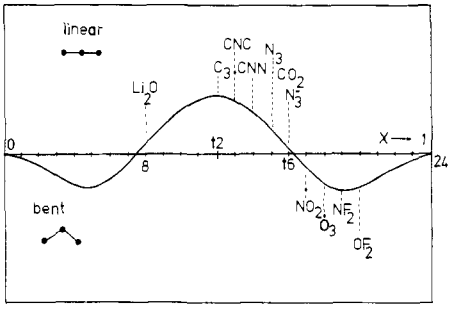

Figure 27. Survey of the geometries of known triatomic molecules. When the curve is above the x axis, linear geometries are predicted; below the x axis bent geometries are predicted.

the bond angle at each atom is much less than 180°. For these systems with $X = 0.75$, bent geometries are predicted (except perhaps for polonium). In the molecular area, many polychalconides are known[26] which appear to be fragments of these chains.

The chain structures of selenium and tellurium may be visualized as distortions of the simple cubic lattice (Figure 24a). In Figure 24b, we show an alternative distortion of the simple cubic lattice which maintains the 180° bond angles around each center. Our preceding discussion suggests that this structure should be less favorable for these elements than the observed one and that the energy difference curve should be determined by the fifth moment difference. Figure 25 shows the calculated energy difference curves for α (observed) and "tetragonal" (unobserved) selenium and tellurium. Once again the early moments successfully anticipate the calculated ΔE functions (Table XIII).

Present evidence for the structures of C_x chains indicates a linear geometry,[27] although for C_3 itself an extremely low bending force

(26) See, for example: Wells, A. F. "Structural Inorganic Chemistry", 5th ed.; Oxford University Press: London, 1984.

(27) The status of the structures of long chains of carbon atoms is reviewed by: Kroto, H. W. *Chem. Soc. Rev.* **1982**, *11*, 435.

Table XV. Effect of Peierls Distortion on Moments

moment	one atom cell (undistorted)	two atom cell ($y = 1.1\beta$)[a]	three atom cell ($x = 1.1\beta$)[a]	three atom cell ($x = 1.2\beta$)[a]	three atom cell ($x = 0.8\beta$)[a]
μ_2	$2\beta^2$	$2\beta^2$	$2\beta^2$	$2\beta^2$	$2\beta^2$
μ_4	$6\beta^4$	$5.912\beta^4$	$6\beta^4$	$6\beta^4$	$6\beta^4$
μ_6	$20\beta^6$	$19.471\beta^6$	$19.698\beta^6$	$18.498\beta^6$	$19.410\beta^6$

[a] See **19** and **20** for the position of the x and y bonds.

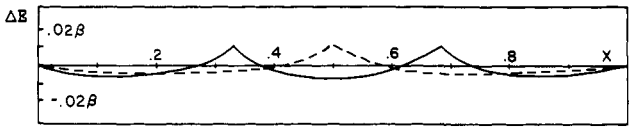

Figure 28. Energy difference curves for various Peierls distortions when compared to the undistorted linear chain. The solid line represents the three-atom Peierls distortion energy difference curves (where $x = 1.1$, see **20**). The dashed line represents the two atom Peierls curve (where $y = 1.1$, see **19**). The line is dashed purely for the sake of clarity.

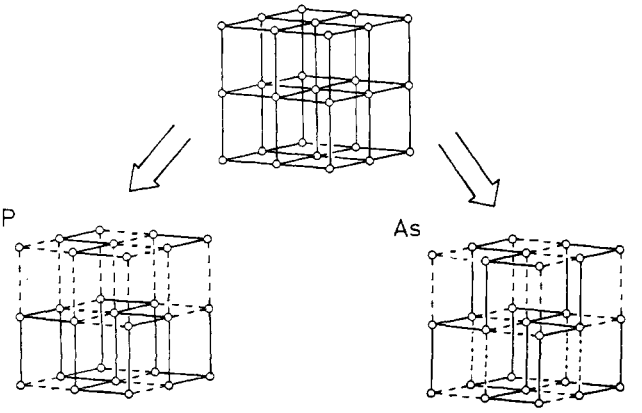

Figure 29. Relation between the arsenic and black phosphorus structures to the simple cubic structure. For further illustrations of the arsenic structure, see also Figure 12 and **44**.

constant is found.[28] Linear geometries are expected from Figure 23. Table XIV shows the calculated moments and Figure 26 shows the results from a complete calculation. $(SN)_x$ forms a Greek-key-type of structure. Its electronic configuration locates it close to a crossing point in Figure 23a. With the heavier sulfur atom its behavior is expected to be intermediate between that of Figures 23a and 23b, and a bent geometry is predicted and observed. The heavier halogens also form chains except that here they are considerably distorted, resulting in both long (intramolecular) and short (intermolecular) distances. Trihalide ions (e.g., I_3^-) are linear, and polyiodides invariably contain mostly linearly coordinated atoms with the inclusion of one or more atoms in a nonlinear environment.[26]

Although in this article we have concentrated on extended arrays, it is interesting to see how Figure 23a matches the observed geometries of first-row triatomic molecules. (A detailed discussion of such molecular problems we reserve for elsewhere). Figure 27 shows where some molecular species would lie on an ideal curve dominated by the fourth moment difference. In addition to homonuclear species we have also included some AB_2 molecules, and so the results at this stage should be viewed with caution. The correlation between the predictions of this paper and those of Walsh's rules is, however, excellent.[29] A Walsh rule "exception", the structure of Li_2O, is in fact fitted by our scheme. The molecule F_3^-, a linear molecule, is predicted to be bent, unlike heavier

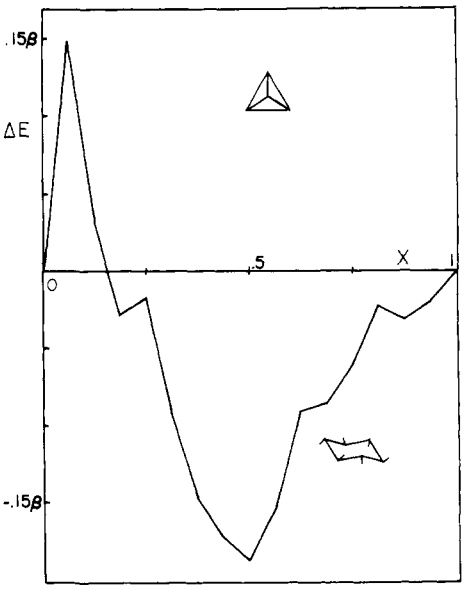

Figure 30. Differences in energy of stabilization by band filling for the α-arsenic and molecular arsenic structures. See Appendix section II for details of the calculation. The energy of α-As was calculated by using the first 30 moments. The molecular As DOS is exact. Since the latter corresponds to a discrete and the former a continuous DOS this curve is not smooth.

analogues such as I_3^-. In fact, from Figure 23, it is only for the first-row trihalide ion that a nonlinear structure is predicted.[30] For heavier elements, the extra lobe generated by the fifth moment difference function allows linear geometries. (Cl_3^-, Br_3^-, I_3^-, and all mixed trihalide ions are indeed linear.) Of particular interest is the movement of the crossing point at about 16.5 electrons in Figure 23a, to lower electron counts with increasing atomic weight. The ion P_3^-, for example, or perhaps As_3^-, an analogue of azide, is predicted to be nonlinear. Perhaps more than anything else, Figure 23 indicates that the so-called Walsh numbers where structural changes are found may in fact depend upon location in the periodic table.

VII. Peierls Distortions

In molecular Hückel theory, one traditionally searches for structures which exhibit large HOMO–LUMO gaps. Large gaps, it is often argued, indicate that the bonding character of the occupied orbitals and the antibonding character of the unoccupied orbitals have been maximized.

Hence, the total energy has been minimized. For example, the Peierls distortion of the linear chain creates band gaps which may stabilize the system. The analogy between Peierls distortions in solids and Jahn–Teller distortions in molecules is one which is often made. In **19** and **20**, we construct the two simplest Peierls distortions. For the dimerization problem (**19**), we examine the effect of increasing every other interaction matrix element along the chain while decreasing the others such that the second moment is identical with that of the parent. (Recall in section III above

(28) Gausset, L.; Herzberg, G.; Lagerquist, A.; Rosen, B. *Astrophys. J.* **1965**, *142*, 45.

(29) A Caveat: Notice that although the crossing point at just over 16 electrons for the AB_2 system is nicely mimicked by the μ_4 curve, a similar plot for an AB_3 system gives the wrong crossing point (at $21^2/_3$ electrons rather than at just over 24 electrons).

(30) A Caveat: We are here applying the results of the infinite chain to the finite molecule. While this application is qualitatively correct, problems may occur. This is especially true as in molecules higher moments can play a substantial role.

the problems associated with comparisons involving second moment changes.) We chose arbitrarily an increase of 0.1β. There

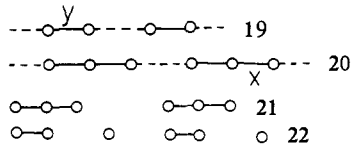

is a choice to be made concerning the interaction matrix elements in the trimerization case—specifically, how are they related in magnitude to the dimerization values. (The fourth moment of this structure remains invariant to such a choice as long as the second moments of **19** and **20** are held equal to that of the parent.) Some ideas as to the values we should use comes from examining the extreme cases (**21** and **22**) where the weaker linkages are completely severed. For $^2/_3$ electron per atom (the case which will interest us), there are two bonding electrons per linkage in **21** but only $^4/_3$ electron per linkage in **22**. As a result **21** has stronger linkages than **22**. We have used values of x (in **20**) equal to 1.2 and 0.8 to show the effect of changing this value. In Figure 28 we show the comparative energies of such systems and in Table XV their first few moments.

We find for this example that the traditional ideas based on Peierls instabilities and the energetic arguments used in this article lead to the same predictions. Figure 28 shows calculated energy difference curves for the parent and two distorted structures. Notice how the curve linking parent and trimer structures is determined by the sixth moment difference. The trimer is therefore stabilized at the $^1/_3$ and $^2/_3$ filled points since it has a smaller sixth moment than the parent. The curve linking parent and dimer is determined by the fourth moment difference. So the dimer is stabilized at the half-filled point relative to the parent since it has a smaller fourth moment.

The instability at the half-filled band for the linear chain has some three-dimensional analogues. We have shown elsewhere how,[17,31] for example, the arsenic and black phosphorus structures may be regarded as broken up simple cubic arrangements (Figure 29). Notice the removal of 4-rings and the emphasis on 6-rings in the structure on distortion away from simple cubic.

VIII. Caveats

There are several areas where our approach does not work. However, to date, these are those areas where Hückel-type ideas fail themselves, rather than where our analysis of the ΔE curves is incompatible with numerical calculation.

We will describe two problems where ideas based upon the rings themselves, while mimicking well the calculated Hückel energy difference curves, are in disagreement with experiment.

In Figure 30 we show the energy difference curve calculated for a pair of structures found for elemental arsenic,[13] namely the sheet structure of Figure 29 and the condensed molecular structure of **23**. The former is more stable in a thermochemical sense, as

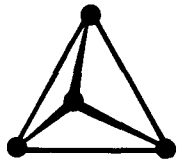

23

is its analogue for phosphorus (black phosphorus). The As_4 tetrahedra are clearly dominated by the 3-rings present in this structure and, by comparison, with the energy difference curve for "tetrahedral" and cubic diamond (Figure 8), we expect the As_4 tetrahedra to be stable relative to the sheets of Figure 29 only at the very beginning of the $\Delta E(X)$ curve. This of course is just what is found in Figure 30. (The moments are shown in Table XVI.) Our energetic arguments lead us to believe α-arsenic (or black phosphorus) is the preferred structure for the group 15 elements (which it is) but also that we would *not* anticipate the existence of As_4 tetrahedra at all. In other words, it should be quite a high-energy species. But, of course, the structure containing such units is known.[32] In this case, HOMO–LUMO arguments appear useful. α-Arsenic is calculated to be semimetallic as a result of a small overlap of filled and empty bands but As_4 is found to have an extremely large HOMO–LUMO gap.

Table XVI. Comparison of Elemental Arsenic Structures[a]

	α-As sheet	As tetrahedra
μ_2	1.0000	1.0000
μ_3	−0.4842	−1.3237
μ_4	2.0256	4.8079
μ_5	−2.1964	−12.3867
μ_6	5.4379	36.9042

[a] As parameters and α-As bond distances were used. Only first nearest neighbors were considered.

The second example concerns the nonexistence of the square (or puckered) S_4 molecule. In section VI we showed that sulfur chains should be bent at each atom and that the preferred bond angle was 90° if μ_4 is maximized. Extending this argument, S_4 squares should be better than S_x spirals since the square itself makes a strong contribution to the fourth moment. However square S_4 molecules are not known. Instead S_4^{2+} (and Se_4^{2+} and Te_4^{2+}) are known in this geometry. Again we calculate for S_4^{2+} a large HOMO–LUMO gap.

Some concluding remarks are in order. The general features of the energy difference curves we have emphasized have been derived from a very simple model where overlap has been ignored in the Hückel sense. Inclusion of overlap will certainly change some of the details of our arguments, especially perhaps at the nearly full band where overlap conspires to greatly destabilize antibonding levels. Another point is our implicit assumption that results for the homoatomic system apply to species where the atoms may have rather different electronegativities. How true this is in general needs to be explored further. In addition it is not yet clear how the discrete nature of the molecular problem will affect our conclusions. (See ref 29 and 30.) All these considerations will influence the location of the crossing points in the ΔE curves.

Acknowledgment. This research was supported by the National Science Foundation under Grants NSF DMR 8019741 and DMR 8216892. We would like to thank Dr. Timothy Hughbanks for helpful discussions.

Appendix

I.1. Hcp and Fcc Structures. The hexagonal close-packed (hcp) and face-centered cubic (fcc) arrangements are two basic structures. Their unit cells may be drawn as in **24**. As may readily

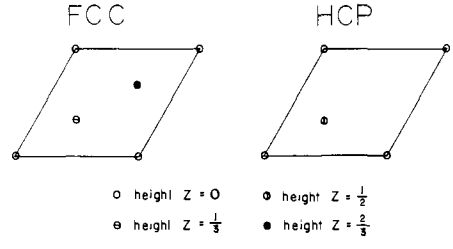

24

be seen (a) any two adjacent layers (viewed down the threefold axis) are geometrically identical for both hcp and fcc. These layers are often drawn to emphasize the octahedral and tetrahedral holes generated by stacking them together, as shown in **25**. (b) It is

(31) (a) Burdett, J. K.; McLarnan, T. J. *J. Chem. Phys.* **1981**, *75*, 5764. (b) Burdett, J. K.; Haaland, P.; McLarnan, T. J. *Ibid.* **1981**, *75*, 5774.

(32) And indeed, too, isoelectronic systems such as *KGe* which contain Ge_4^{-4} tetrahedra (Busman, E. *Z. Anorg. Chem.* **1961**, *313*, 90).

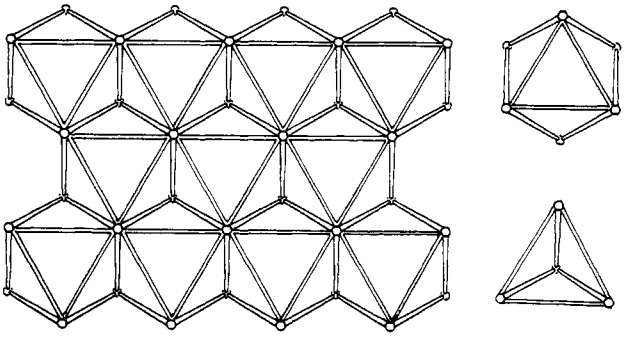

25

the addition of the third layer which distinguishes the two structures from each other. Referring to the unit cells of **24**, one finds that the third layer in hcp lies in an eclipsed fashion over the first two layers (**26**), while in fcc it lies in a staggered fashion

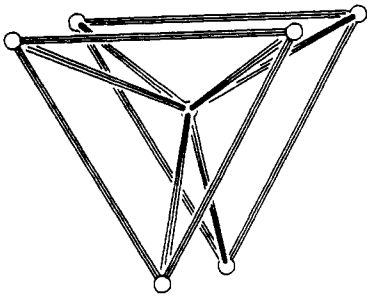

26

(**27**). The third layer is drawn in the diagrams of **28** and **29** to

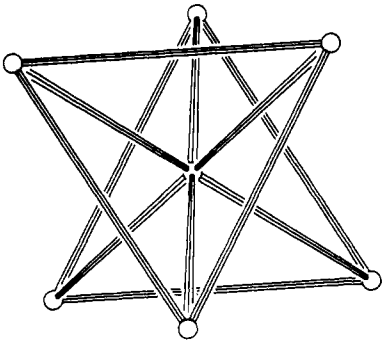

27

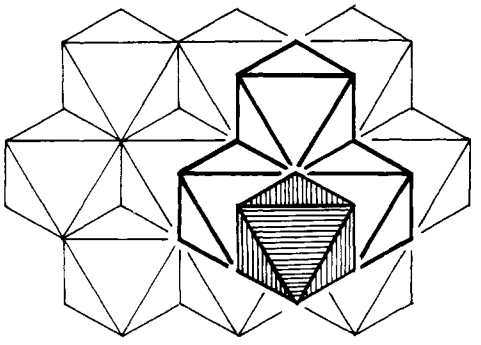

28

give the fcc and hcp arrangements, respectively. In **30** we show how the octahedra in fcc share faces only with tetrahedra. In contrast the octahedra in hcp also share faces with adjacent octahedra (**31**). Tetrahedra in hcp also share faces with other tetrahedra (**32**).

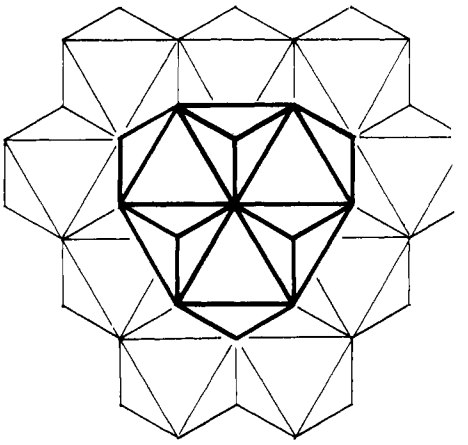

29

2. Comparison of Hcp and Fcc Moments. Within any two adjacent layers (viewed down the threefold axis), the fcc and hcp

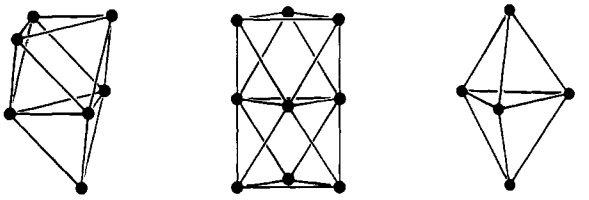

30 31 32

stackings are identical. Thus, for hcp and fcc to have nonidentical walks, at least three layers must be involved. If only nearest-neighbor interactions are considered, a path which involves three layers must be at least of length 4. This is true irrespective of the type of orbital used to populate each vertex.

s Orbitals Only. If each vertex is populated with a single s orbital, a rather interesting result is found; fcc and hcp have identical nth moments, for all n, and hence they have identical energy densities of states. This was first observed by Cyrot-Lackmann. We now prove her result.

Let 0_i and 0_j be two atoms in the same threefold (close-packed) layer which we will call an 0 layer. Let, for example

$$[(0_j1212321)0_i]_{\text{fcc or hcp}} \qquad \text{(A.1)}$$

represent the number of paths which connect 0_i and 0_j which involve a pattern of steps between layers shown pictorially in **33**.

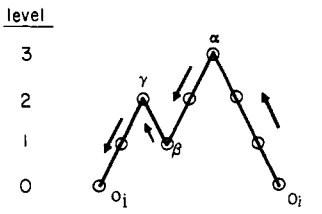

33

Thus the only paths which count toward expression 1 are those which march directly upward for three steps to reach an arbitrary point α in the layer 3, march down two steps to reach some atom β in layer 1, up again one step to reach γ, and finally down two steps to reach 0_j.

Now in the case of fcc, the only types of allowed upward steps are a_1, a_2, and a_3, while the only allowed downward steps are a_1^{-1}, a_2^{-1}, and a_3^{-1} where these vectors are shown in **34**. For hcp,

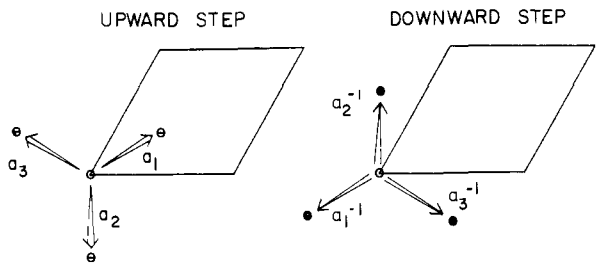

34

depending whether one is on an even or odd layer, there are different possible steps shown in **35** and **36**.

We now note three geometrical facts, which, when placed side by side, will prove our assertion. (a) In **33**, each layer is crossed an even number of times. This is clearly true for any path which

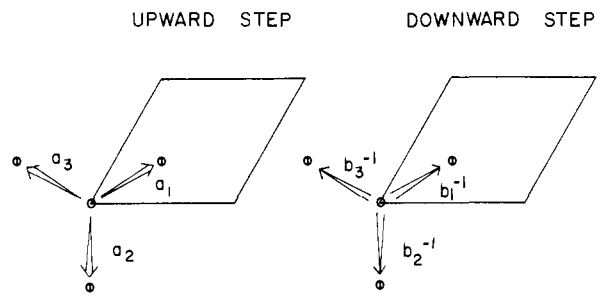

35

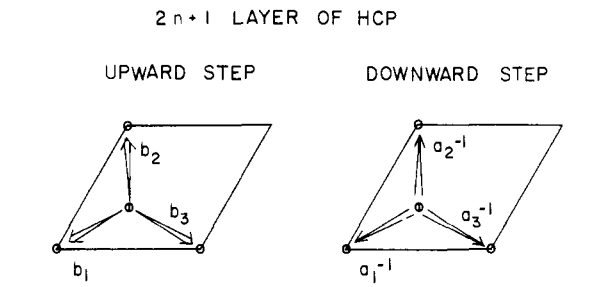

36

connects 0_i and 0_j. (b) When moving from any layer (label it m) in hcp to an adjacent layer ($m + 1$), one must take an a_i step, and on moving from $m + 1$ to m, one must take an a_j^{-1} step (i is not necessarily equal to j). (c) If the path of **33** is viewed projected by the xy plane, Proj(b_i^{-1}) = Proj(a_i) while Proj(b_j) = Proj(a_j^{-1}).

Let us now relabel **33** with a_i's for the case of an fcc lattice as in **37**. The corresponding "equivalent" hcp path must be of the form shown in **38**, where we have not as yet made any con-

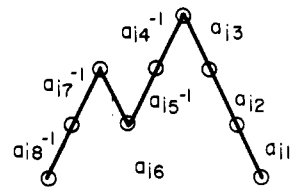

37

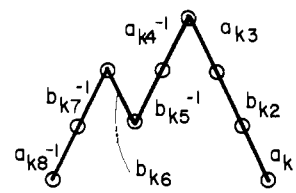

38

nection between the k_n indexes of the hcp system and the i_m indexes of the fcc system. We represent 0_j with a question mark since it is not yet obvious perhaps whether we can ever reach 0_j in the hcp system.

We now introduce the connection between the i_m and k_n indexes. Wherever the walk is between an odd layer on top (positive z) and an even layer below, let $a_{ij} = a_{kj}$. Whenever the step between two layers of which the topmost is even, invert the k_n indexes of that layer in a pairwise fashion. Thus, between layers 1 and 2, there are four steps, a_{i2}, a_{i5}^{-1}, a_{i6}, and a_{i7}^{-1} and b_{k2}, b_{k5}^{-1}, b_{k6}, and b_{k7}^{-1}. We set $i2 = k5$, $i5 = k2$, $i6 = k7$, and $i7 = k6$. Such a transformation assures us of reaching 0_j. Furthermore it establishes a one-to-one correspondence in paths of hcp and fcc, albeit with the restriction our paths may not (as yet) include steps which do not leave the threefold planar sheets. This restriction may easily be lifted by noting that fcc and hcp are identical within each close-packed layer, and thus any planar step in fcc can always be mimicked by the same planar step in hcp (and vice-versa). This maintains our one-to-one correspondence in fcc and hcp for all paths which link two atoms belonging to the same layer. For example, let **39** represent the six possible planar steps. Then the

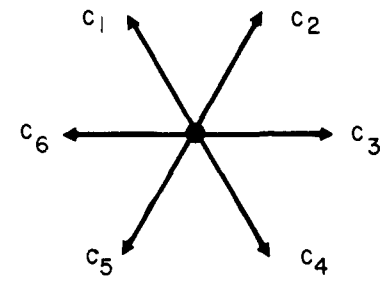

39

sample path for fcc becomes that shown in **40** and the corresponding hcp path that shown in **41**. These two diagrams show

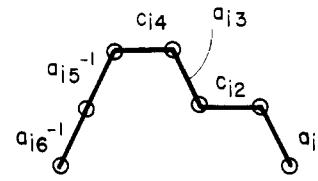

40

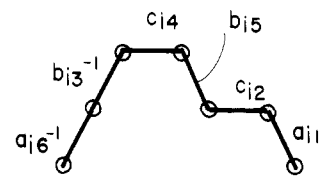

41

the one-to-one correspondence between paths connecting two atoms lying in the same threefold layer. We are interested in returning walks only, namely the case $0_i = 0_j$. This type of result may be extended to other systems.

We are now in a position to examine the Cyrot-Lackmann result that all close packings have equivalent nth moments when each node is populated with a single s orbital, and hence all such close packings have identical densities of states. From the point of view of the threefold axis, any two adjacent layers in any close packing are connected either in the a_i fashion or in the b_i fashion of **36**. A mapping which transforms the paths of an arbitrary close packing in a one-to-one fashion into those of an fcc packing is one which leaves all steps of the a_i type unchanged but reverses all b_i steps in the pairwise fashion described for hcp. Since the interaction integrals between s orbitals are isotropic, this makes no difference to the weight of the walk in the evaluation of μ_n.

3. Related Structures. Fcc and hcp lattices are not only interesting in their own right but also because, by filling the octahedral and tetrahedral holes of these structures, other crystal structures are generated. Perhaps the best known of such filled-up variants are the wurtzite and sphalerite structures or, if all the atoms are of the same species, of hexagonal (lonsdaleite) and cubic diamond. These are generated by filling one-half of the tetrahedral holes of the parent lattices as in **42** and **43** such that the inserted

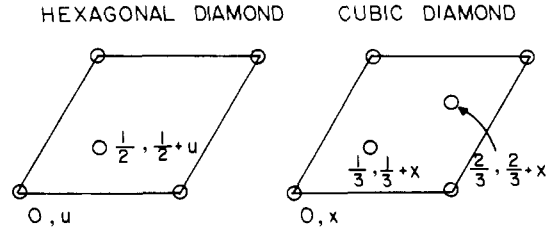

42 43

Table XVII. Symmetry Equivalences in 5-Cycles in Close-Packed Structures

$[0_i0121]$	A/2
$[0_i0,1,0,-1]$	B/2
$[0_i0,-1,-2,-1]$	A/2
$[0_i0,-1,0,1]$	B/2
$[0_i1221]$*	A/2
$[0_i1211]$	B/2
$[0_i1210]$	A/2
$[0_i1121]$	B/2
$[0_i1,1,0,-1]$	A/2
$[0_i1,0,0,-1]$	B/2
$[0_i1,0,-1,0]$	B/2
$[0_i1,0,-1,-1]$	A/2
$[0_i-1,-2,-2,-1]$*	A/2
$[0_i-1,-2,-1,-1]$	B/2
$[0_i-1,-2,-1,0]$	A/2
$[0_i-1,-1,-2,-1]$	B/2
$[0_i-1,-1,0,1]$	A/2
$[0_i-1,0,0,1]$	B/2
$[0_i-1,0,1,0]$	B/2
$[0_i-1,0,1,1]$	(A/2)/[(5A) + (5B)]

Table XVIII. Contributions to μ_5[a]

	no. of cycle I	no. of cycle II	tot[c]
type 1[b]	12	0	60
type 2	6	0	30
type 3	0	6	30
type 4	0	6	30
type 5	12	0	60
unit α[d]	0	6	30
unit β	6	0	30

[a] Irrespective of whether the structure is fcc or hcp. [b] These paths are shown in Figure 31. [c] We know from Table XVII that there are five cycles of each type. [d] These paths are shown in Figure 32.

Table XIX. Contributions to μ_4

		fcc	hcp
type a[a]	planar 4-ring (θ = 120°)	24	
	puckered 4-ring (θ = 99.6°)		24
type b	three atom chain (φ = 180°)	12	
	three atom chain (φ = 99.6°)		12
type c	three atom chain (φ = 120°)	24	
	three atom chain (φ = 146.4°)		24

[a] Walks of these types are shown in **48**.

atoms themselves form a close-packed lattice of the same type. We suggest that hexagonal and cubic diamond have equivalent $\{\mu_n\}$ when each atom is populated with a single s orbital and hence have identical energy densities of states. This may be seen in the following way. Both structures are composed of tetrahedral four-connected nets based on interconnected puckered graphite sheets as in **44**. It is most convenient to conceptually unpucker

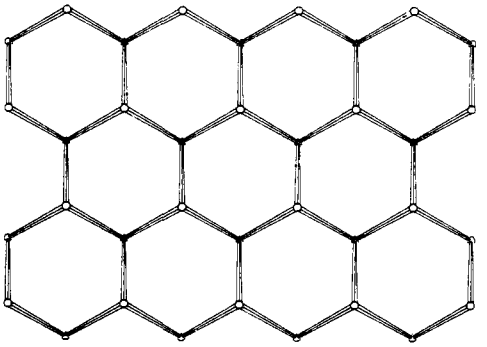

44

such sheets. (The walks remain unchanged.) It is then these graphite sheets which will take the place of the two-dimensional close-packed sheets of the preceding examples. The chief difference here is that a single graphite sheet contains two sorts of

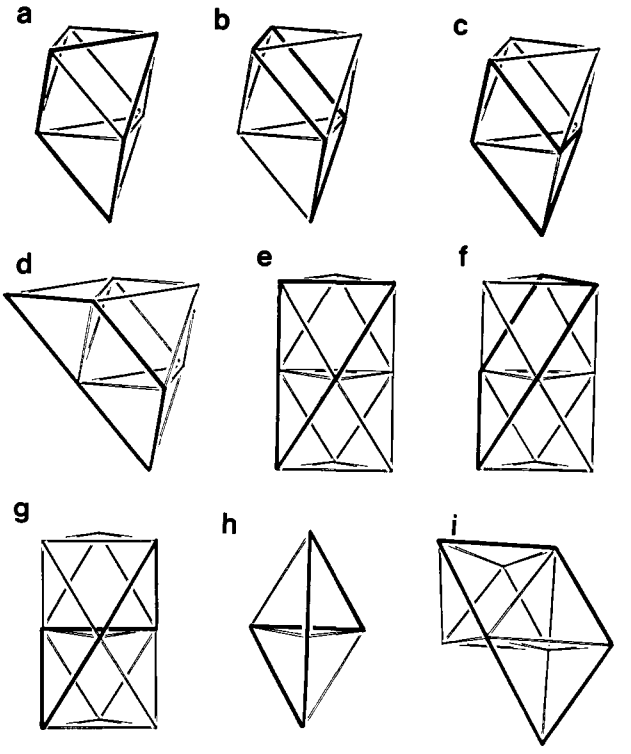

Figure 31. Darkened lines in (a)–(i) represent the five-membered rings present in fcc and hcp. (a)–(d) represent, respectively, the type 1, 2, 3, and 5 paths for the fcc structure enumerated in Table XVIII. It should be noted (c) also forms the type 4 fcc path. (We have made this division to simplify comparison with the hcp structure.) (e)–(i) form the type 1, 2, 3, 4, and 5 paths for the hcp structure enumerated in Table XVIII.

atoms, unlike the close-packed case. We will use α_i and a_i to refer to the steps permitted respectively from the "Greek" and "Roman" atoms of **45**. For all layers in cubic diamond, the Roman atoms

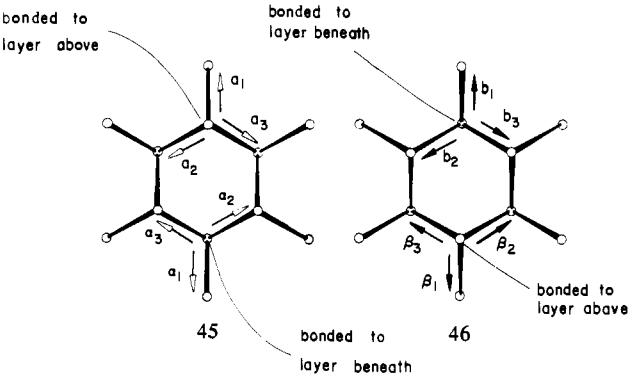

of one layer are coordinated to Greek atoms of the layer above (and vice-versa), with a_i and α_i vectors of the same type. In hexagonal diamond, only even layers are composed of atoms whose nearest neighbors are reached via a_i and α_i vectors. For odd layers, we need to introduce (**46**) the vectors b_i and β_i, related to those f **45** by a simple rotation. The atoms of **45** and **46** behave similarly for walks which do not leave the layer.

The proof of our statement concerning identical nth moments for s orbital based cubic and hexagonal diamond lattices relies on the following observations.

(a) In any path which goes from the 0 layer to the 2 layer, one more b_i step is taken than β_i step. In any path which goes from the 2 layer to the 0 layer, one more β_i step is taken than b_i step.

(b) In any path which goes from the 0 layer to the 1 layer and back to the 0 layer, an equal number of b_i and β_i steps are taken.

We now show that there exists a one-to-one correspondence of paths which connect two atoms (0_i and 0_j) of the 0 layer. This

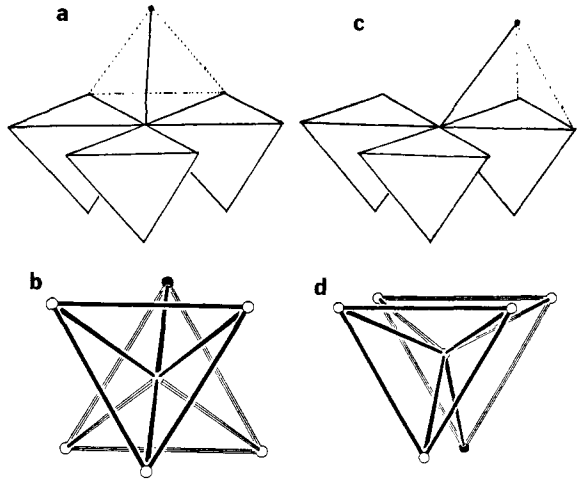

Figure 32. μ_5 contributions to the fcc and hcp structures which arise from a three-membered ring coupled to a neighboring atom. It is convenient to group such contributions into a single geometrical unit. In (a) and (b), we illustrate for fcc two simple units which in conjunction account for all paths of this type. The fifth moment of the circled atom in (a) and (b) represent, respectively, "unit α" and "unit β" of Table XVIII. (c) and (d) form, respectively, the "unit α" and "unit β" for hcp.

must be so since any path must cross a given sheet an even number of times and, with (a)–(c) above, there are for any given layer an equal number of b_i and β_j and similarly an equal number of a_i and α_i steps. Just as before, our one-to-one transformation is achieved by leaving the a_i and α_i steps and the extra-layer steps unchanged while reversing the indexes on the b_i and β_i steps. Finally we set $0_1 = 0_j$.

4. μ_5 for Hcp and Fcc Lattices. As shown above, for a path to exhibit a different structure in fcc compared to hcp, it must traverse at least three layers (viewed parallel to the threefold axis). When the starting layer of the walk is denoted as layer 0 and the layers above and below it as 1 and −1, respectively, a sample path may be viewed in the pictorial fashion of **47**, where I_i is a specific

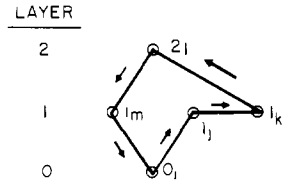

47

atom in layer I and the lines indicate nearest-neighbor contacts. Such a path contributes equally to the fifth moment for each atom (orbital) in the loop. As we noted before, this is reminiscent of permutation cycles, and we therefore label the contribution of the above path to the fifth moment $[0_i1_j1_k2_i1_m]$. We wish here to find all nonzero 5-cycles. To do so, it is convenient to group the 5-cycles in the following manner. Let

$$[0_i1121] = \sum_{j,k,l,m} [0_i1_j1_k2_i1_m]$$

This sum is the contribution of all paths which start at atom O_i on level 0, jump to level 1 in the first step, stay on level 1 in the second step, jump then up to level 2, and, finally, in the last two steps, return to level 0. Table XVII lists all the nonzero sums of cycles of this form. We have eliminated all 5-cycles which do not traverse three layers and all 5-cycles which do not move between connected atoms in adjacent layers. We now wish to find which of the 20 remaining 5-cycles are symmetry-equivalent. Before enumerating the symmetry operations we note that our example $[0_i1121]$ does not appear, as written, to be truly cyclic. This is because 0_i refers to a specific atom on a specific layer while 1, 1, 2, and 1 refer to layers only. Therefore, we consider

$$[01121] = \frac{1}{N}\sum_i [0_i1121]$$

where N is the number of atoms in the 0 layer and the crystal is regarded as being extremely large but finite. As all atoms in a given layer for both hcp and fcc are translationally equivalent

$$[0_i1121] = [0_j1121] \quad \text{for all } i \text{ and } j$$

and so

$$[01121] = \frac{N}{N}[0_i,1,12,1] = [0_i1121]$$

We can now enumerate the symmetry operations. (1) [01121] = [11210]. As the sum of cycles have the cyclical behavior of true cycles, we may put any element as the first element in the row. (2) [01121] = [01211]. Every cycle contributes to the fifth moment with the same weight as its inverse. In one case, the loop is traversed in a clockwise and in the other in a counterclockwise fashion. (3) [01121] = [0,−1,−1,−2,−1]. For fcc each atom has an associated inversion center. In hcp each atom lies in a σ_h mirror plane. All the signs of the cycle may therefore be changed. (4) [01121] = [−10010]. Any integer may be added to the cycle. In the case of fcc this is due to the translational symmetry. In the case of hcp this is due to the presence of screw axes.

Using these symmetry relationships, we find that there are only two different classes of cycles which we label accordingly: cycle I [01221] ≡ A/2; cycle II [01121] ≡ B/2. In Table XVII, the collection of cycles are classified in this way. We include the factor of $^1/_2$ to remind ourselves that it is paths which we are counting and not rings.

By direct counting we find, with reference to Figures 31 and 32, the results of Table XVIII.

5. μ_4 for Hcp and Fcc. In contrast to μ_5, the paths of length 4 are fewer and much easier to visualize and to count. In the notation of the previous section, there are only four 4-cycles: $[0_i121]$, $[0_i,-1,-2,-1]$, $[0_i,1,0,-1]$, and $[0_i,-1,0,1]$. All 4-cycles are equivalent. We enumerate their paths in Table XIX.

6. Numerical Differences in μ_4 and μ_5. In Table XX we calculate the differences in μ_4 and μ_5 for the fcc and hcp lattices for the all p and all d cases. For the pure p situation, the

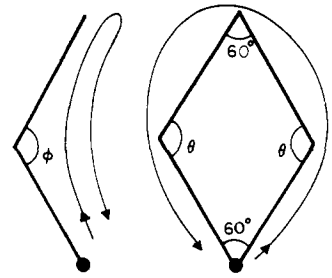

48

difference in μ_4 between fcc and hcp comes from the puckering of the 4-ring in going from fcc to hcp. The effects of twists in the bonds largely cancel themselves out, leading to a small difference in μ_4 between the two structures. It is the μ_5 difference which determines the final shape of the ΔE curve. $|\mu_5|$ is larger for hcp, and the difference is due entirely to the different conformations of the 5-rings present in the two structures.

Exactly the opposite result is found for the d-orbital case, and $|\mu_5|$ is larger for the fcc structure. As may be seen from Figure 16, higher moments are also important in controlling the energy difference curve in this case. The analysis of this problem in general, by enumeration of the 6-rings and 7-rings, is not particularly revealing.

II. As described earlier, the Hückel method (as defined in ref 2) was used in all calculations. The atomic parameters used are given in Table XXI. Exponents listed in Table XXI are Slater-type orbital exponents. All calculations were done by using the single ζ expansion.

In the calculations involving carbon and boron structures, i.e., the results shown in Figures 4, 8, 9, and 26, carbon parameters were used. For Figures 4 and 26, the calculations on three-co-

Table XX. Numerical Evaluation of μ_4 and μ_5 Contributions

		d orbitals		p orbitals	
type of struct	tot no.	μ_5 (hcp-fcc) per unit	total μ_5(hcp-fcc)	μ_5 (hcp-fcc) per unit	total μ_5(hcp-fcc)
			a.		
1	60	-4.26×10^{-4}	-2.55×10^{-2}	6.75×10^{-5}	4.10×10^{-3}
2	30	8.02×10^{-4}	2.40×10^{-2}	-3.55×10^{-4}	-1.07×10^{-2}
3	30	-7.98×10^{-4}	-2.40×10^{-2}	6.75×10^{-5}	2.05×10^{-3}
4	30	6.90×10^{-4}	2.07×10^{-2}	-4.98×10^{-4}	-1.50×10^{-2}
5	60	6.79×10^{-4}	4.08×10^{-2}	-2.26×10^{-4}	-1.36×10^{-2}
α	30	-8.45×10^{-4}	-2.54×10^{-2}	0	0
β	30	1.21×10^{-3}	3.64×10^{-2}	0	0
total			4.71×10^{-2}		-3.31×10^{-2}
			b.		
a	24	-4.91×10^{-4}	-1.19×10^{-2}	5.39×10^{-4}	1.26×10^{-2}
b	12	-8.35×10^{-3}	-1.00×10^{-1}	-1.48×10^{-2}	-1.77×10^{-1}
c	24	3.86×10^{-3}	9.27×10^{-2}	7.38×10^{-3}	1.77×10^{-1}
total			-1.96×10^{-2}		1.26×10^{-2}

Table XXI. Atomic Parameters

valence orbital	H_{ii}, eV	ζ
C 2s	−21.4	1.625
C 2p	−11.4	1.625
As 4s	−20.0	2.230
As 4p	−9.5	1.890
Se 4s	−20.0	2.440
Se 4p	−9.5	2.070
Te 5s	−17.1	2.500
Te 5p	−8.6	2.200
Bi 6p	−10.0	2.100
all transition metals		
3d	−10.0	2.100

ordinate planar nets and on infinite carbon chains, the C–C distance was 1.42 Å and only first nearest-neighbor interactions were considered. For results involving comparison with the diamond structure (Figures 8 and 9), a C–C bond distance of 1.54 Å was used. Thus, in Figure 9 in the comparison of the diamond and the rhombohedral boron structure the atomic density of 5.62 Å^3/atom was considered. In this last calculation, we considered only bonds whose distances were shorter than 2.0 Å which effectively limits the calculation to first nearest neighbors.

For the results on fifth-row main group compounds, Bi parameters were used throughout. α-Bi first and second nearest-neighbor distances were, respectively, 3.07 and 3.53 Å, these being the experimentally observed ones. To maintain constant density, we set fcc bonds at 3.69 Å and α-Po distances at 3.28 Å. For both the fcc and α-Po structures only, first nearest neighbor interactions were included, while for α-Bi both first and second nearest-neighbor interactions were included.

For the work on Te and Se (Figure 25), we used in all cases the experimentally observed bond distances in both α-Te and α-Se. α-Se has first and second nearest neighbors at 2.37 and 3.44 Å, respectively, while α-Te has bond distances of 2.83 and 3.49 Å. Only first and second nearest-neighbor interactions were included in these calculations.

In the As calculation shown in Figure 30, we used the experimentally observed bond distances found in α-As (which is 2.52 Å) for both structures considered. Only first nearest-neighbor interactions were included.

Finally the transition-metal calculations (Figures 16 and 21) were based on a d-orbital-only model with the chosen atom loosely based on Fe and we assumed a density (all calculations were done at the density of 11.2 Å^3/atom) similar to Fe. This assumption leads to a first and second nearest-neighbor bond distances in bcc of 2.44 and 2.82 Å, respectively, an fcc nearest-neighbor distance of 2.51 Å, and a simple cubic nearest-neighbor distance of 2.24 Å. In both the fcc and simple cubic case, only first nearest-neighbor interactions were included. For bcc, both first and second nearest-neighbor interactions were included.

In this last paragraph we would like to identify the meaning of β used in the above calculations. In the results shown in Figures 4, 8, and 10, β equals the maximum cohesive energy per atom of the diamond structure (i.e., the cohesive energy at the most favorable electron count). In Figures 16 and 21, β represents the maximum cohesive energy per atom of the bcc structure. In the fifth-row main group calculations, β equals α-Bi's greatest cohesive energy per atom. For the calculations of Figures 25, 26, and 30, β was set according to the α-Se, linear carbon chain and α-As structures, respectively.

(33) The group notation is being changed in accord with recent actions by IUPAC and ACS nomenclature committees. A and B notation is being eliminated because of wide confusion. Group I becomes groups 1 and 11, group II becomes groups 2 and 12, group III becomes groups 3 and 13, etc.